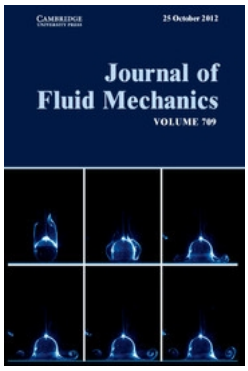

Instabilities in a high-Reynolds-number boundary layer on a film-coated surface

S. N. TIMOSHIN

Journal of Fluid Mechanics / Volume 353 / December 1997, pp 163 - 195
DOI: 10.1017/S0022112097007337, Published online: 08 September 2000

J. Fluid Mech. (1997), *vol.* 353, *pp.* 163–195. Printed in the United Kingdom

Instabilities in a high-Reynolds-number boundary layer on a film-coated surface

By S. N. TIMOSHIN

Department of Mathematics, University College London, Gower Street, London WC1E 6BT, UK

(Received 13 June 1996 and in revised form 12 February 1997)

A high-Reynolds-number asymptotic theory is developed for linear instability waves in a two-dimensional incompressible boundary layer on a flat surface coated with a thin film of a different fluid. The focus in this study is on the influence of the film flow on the lower-branch Tollmien–Schlighting waves, and also on the effect of boundary-layer/potential flow interaction on interfacial instabilities. Accordingly, the film thickness is assumed to be comparable to the thickness of a viscous sublayer in a three-tier asymptotic structure of lower-branch Tollmien–Schlichting disturbances. A fully nonlinear viscous/inviscid interaction formulation is derived, and computational and analytical solutions for small disturbances are obtained for both Tollmien–Schlichting and interfacial instabilities for a range of density and viscosity ratios of the fluids, and for various values of the surface tension coefficient and the Froude number. It is shown that the interfacial instability contains the fastest growing modes and an upper-branch neutral point within the chosen flow regime if the film viscosity is greater than the viscosity of the ambient fluid. For a less viscous film the theory predicts a lower neutral branch of shorter-scale interfacial waves. The film flow is found to have a strong effect on the Tollmien–Schlichting instability, the most dramatic outcome being a powerful destabilization of the flow due to a linear resonance between growing Tollmien–Schlichting and decaying capillary modes. Increased film viscosity also destabilizes Tollmien–Schlichting disturbances, with the maximum growth rate shifted towards shorter waves. Qualitative and quantitative comparisons are made with experimental observations by Ludwieg & Hornung (1989).

1. Introduction

Laminar boundary layers on aircraft wings and turbine blades or on the walls of a channel or pipe tend to become unstable at a sufficiently high flow speed. When the solid flow boundary is coated with a thin film of a different fluid, the film and the main boundary layer turn into a complex fluid-dynamical system showing a fascinating pattern of instabilities and nonlinear behaviours, often with dramatic changes in the flow properties due to the film rupture, the formation of interfacial waves, droplets and aerosols. All this is in addition to laminar–turbulent transition in the boundary layer, or in the film, or in both.

Our concern in this paper is with linear instability of boundary-layer flows on film-coated surfaces such as on a rain-wetted car or airplane wing; related examples are found in film cooling technologies, in lubricating pipelining, and in visualization experiments. The characteristic Reynolds number in the flow is assumed to be large, as is typical in many applications. We use asymptotic analysis to examine the flow regimes arising when a relatively thin film affects the stability of the main flow and

vice versa, with the emphasis on the situations where the two flows are strongly coupled by virtue of the interfacial stress and velocity continuity.

The linear stability problem for a viscous flow along an interface between two immiscible fluids with different viscosities and densities was introduced by Lock (1954) and Feldman (1957), the former in the context of water-wave generation by wind, and the latter for a shear-driven film flow similar to that considered in this paper; in both cases the flow stability was found to be strongly influenced by the interface (however, the qualitative conclusions in those papers were later shown to be impaired by errors in the interfacial conditions). The continuing development of the instability theory for such flows relies, even today, on analytical and numerical approaches, some of which will be reviewed here.

At high Reynolds numbers, the flow of a light fluid over a sufficiently thick coat of a heavier and more viscous substance (as in an air/water combination) can become unstable to inviscid Rayleigh-type disturbances (Miles 1957; see also Morland, Saffman & Yuen 1991; Morland & Saffman 1993; Shrira 1993). Dealing mostly with the problem of water-wave generation by turbulent wind Miles (1959, 1962) and Benjamin (1959) extended the inviscid-flow model by including some of the viscous effects and hence derived an estimate for the critical Reynolds number (or the critical wind speed) for the incipient instability. These approximate theories were compared with accurate numerical solutions for the full viscous formulation by Valenzuela (1976) and, more recently, by van Gastel, Janssen & Komen (1985) and Belcher, Harris & Street (1994), who indicate also that the results can be rather sensitive to the turbulence model used for the mean profiles in air and in water.

For entirely laminar basic flows the choice of the mean profile can be put on a firmer basis (in theory at least) and the effect of various factors on the flow stability can be assessed more systematically. The significance of the viscosity difference at the interface was demonstrated by Yih (1967) in his analysis of a long-wave mode of viscous instability in a Poiseuille–Couette channel flow. Yih showed that a relatively thin coat of a more viscous fluid on one of the channel walls renders the flow unstable at small and $O(1)$ Reynolds numbers, which contrasts with the ultimate linear stability of Couette flow and the low-Reynolds-number stability of Poiseuille flow without wall coating. The viscosity difference and hence a slope discontinuity in the velocity profile also accounts for a short-wave viscous instability present at all Reynolds numbers, see Hooper & Boyd (1983), and Blennerhassett & Smith (1987). A short-wave cut-off of such growing modes is usually due to surface tension.

The growth rates of long waves in Yih's (1967) channel flow are of $O\left(k^2\right)$ (where $k \ll 1$ is a non-dimensional disturbance wavenumber) and depend on the fluid densities and the relative amount of the more viscous fluid, as was demonstrated further by Blennerhassett (1980), Renardy (1985) and Yantsios & Higgins (1988). The last three papers also present an extensive computational study in the part of the wavenumber–Reynolds number parameter plane inaccessible to asymptotic techniques and discuss the significance of two varieties of growing modes corresponding to the interfacial and Tollmien–Schlichting (TS) or shearing instability (a possible interplay of the two modes was noticed earlier by Miles 1962). For the flow regimes chosen by Blennerhassett (1980) the TS waves appear at far larger Reynolds numbers and generally look much weaker than the interfacial mode. A competition between the two instabilities is more evident for the channel flows studied in Yantsios & Higgins (1988); it is also reflected in their comparisons with experiments by Charles & Lilleleht (1965), and Kao & Park (1972). For flow of the Lock (1954) type Akylas (1982) proposed a linear TS/interfacial mode resonance as a mechanism of water-wave generation.

When, in the case of a two-layer channel flow, the thickness of one layer becomes sufficiently small, the influence of the opposite solid boundary can be neglected provided that the disturbance wavelength remains comparable to the film thickness. We arrive then at the stability problem for a linear-profile film driven by a constant-shear unbounded flow (under certain assumptions the same limiting formulation holds also for the boundary-layer flows considered in this paper). Owing to the absence of the second rigid wall the growth rate of Yih's (1967) long-wave instability in strongly viscous films changes from $O\left(k^2\right)$ to $O\left(k^{4/3}\right)$ at small k, Hooper (1985). For the same flow Hooper & Boyd (1987) described a new type of high-Reynolds-number instability when the kinematic viscosity of the unbounded fluid is large. We emphasize that the constant-shear approximation for the basic-state profile predicts only interfacial instability which, depending on circumstances, consists of one or two neutral branches. It is interesting that the most common combination of two immiscible fluids in nature, namely air and water, turns out to be rather complex, for the large water density and viscosity support long interfacial waves, whereas the relatively large kinematic viscosity of air gives rise to a short-wave interfacial mode. For a thin water layer driven by an air current a useful limiting instability formulation is that of a liquid film with a free surface (Miles 1960; Smith & Davis 1982). Related problems have been studied extensively in the context of free-falling or gravity-driven films on sloping walls; for a recent review see Chang (1994). Some aspects of the problem were also examined within the high-Reynolds-number asymptotic framework akin to that in the present paper, in both steady (e.g. Gajjar & Smith 1983; Gajjar 1987; Bowles & Smith 1992; Bowles 1995) and unsteady (e.g. Mahmudov & Terent'ev 1988; Brotherton-Ratcliffe & Smith 1989; Bagbekov & Terent'ev 1991; Hoyle & Smith 1994) formulations. Subtle differences between the purely free-surface and the limiting shear-driven flows are discussed by Miesen & Boersma (1995). As a separate, but potentially related and extremely interesting application, we should also mention problems involving the film formation due to condensation, for example on inclined cold walls placed in a saturated vapour stream; see Beckett & Poots (1972), Howarth, Poots & Wynne (1978), Shu & Wilks (1995).

The linear stability analysis reported in this paper is a part of research directed eventually at weakly and strongly nonlinear theoretical modelling of transitional boundary layers on wave-supporting liquid coatings. This determines the use of a high-Reynolds number approach and the specific scalings assumed in the flow. Since the boundary-layer flow, whether on a solid or film-coated surface, is generally non-parallel the use of a parallel-flow Orr–Sommerfeld approximation (and of the classical Heisenberg–Tollmien type of asymptotic analysis; see e.g. Lin 1955) becomes particularly vulnerable from a theoretical standpoint (this does not diminish their value in certain, for instance engineering, applications). What is more important is that when taken into nonlinear regimes, such essentially finite-Reynolds-number theories come across severe mathematical difficulties which almost invariably overshadow the underlying physics. An alternative adopted in this study is a multi-deck analysis developed by Neiland (1969), Stewartson & Williams (1969) and Messiter (1970) for application to flow separation and widely used in instability theory since the work of Smith (1979*a*,*b*) in the West and Zhuk & Ryzhov (1980) in Russia. Subsequent developments in this area are summarized in the review articles by, e.g., Stewartson (1974), Smith (1982), Messiter (1983), and Cowley & Wu (1993).

The multi-deck approach is less demanding on the computational side and hence leads to tractable formulations even in multi-parameter problems like the one considered in this paper. In practical terms it often produces amazingly accurate results

at realistic Reynolds numbers; see for example recent comparisons by Smith & Bowles (1992), Stewart & Smith (1992), Hultgren (1992), and Healey (1995). One should be fully aware of limitations of the multi-deck theory stemming from the fact that certain properties of the instability spectrum at finite Reynolds numbers can be quite different from their high-Reynolds-number counterparts, both qualitatively and quantitatively (see, e.g., Healey 1995; Timoshin 1996). Clearly a joint effort with computationalists and experimentalists is required to produce a physically sensible and formally acceptable theory. The analysis in this paper focuses on the asymptotic flow properties.

In a flat-plate boundary layer without coating the most amplified TS disturbances appear near the lower neutral branch; see, e.g., Ryzhov & Terent'ev (1986). The wavelength and time scale for such waves are of order $Re^{-3/8}$ and $Re^{-1/4}$ respectively (in terms of the Reynolds number Re and non-dimensional variables based on the global parameters specified below in §2). One of the dynamically active elements of the TS-wave structure is a near-wall viscous layer of non-dimensional thickness $O\left(Re^{-5/8}\right)$. The disturbance viscous layer is therefore much thinner than the $O\left(Re^{-1/2}\right)$ main boundary layer. The lower-branch TS waves are slow, their phase speed is an $O\left(Re^{-1/8}\right)$ fraction of the free-stream velocity. In order to examine the effect of a wall coating on the TS instability we shall assume the film and the TS-wave viscous layer to be of comparable thickness (the assumption seems appropriate since sufficiently far away from the region of film generation the film becomes asymptotically thin compared to the boundary layer; see Nelson, Alving & Joseph 1995). The equations derived on this basis are found to describe both the TS waves of the main boundary layer modified by the film and interfacial waves. The interfacial modes covered by the model are of two kinds: long waves propagating somewhat faster than the unperturbed interface (as in Yih 1967), and shorter-scale disturbances travelling slower than the interface (as in Hooper & Boyd 1987). We examine how these waves are affected by the viscous/inviscid interaction in the main boundary layer.

A related triple-deck approach is being developed by Tsao, Rothmayer & Ruban (1997) with application to the airplane de-icing technology (for an earlier study on the subject see, e.g., Yih 1990). The crucial simplifying assumption used in that work is the extremely large viscosity and density of the de-icing liquid. This leads to a somewhat simpler viscous/inviscid interaction problem, with the TS instability excluded from analysis.

The plan of the paper is as follows. In §2 the flow geometry is introduced and the equations of viscous/inviscid interaction in a two-fluid flow are derived for the general case of nonlinear disturbances. In §3 the interaction equations are linearized and solved for the TS and interfacial temporal instability modes in a range of flow parameters. Viscosity and density variation at the interface as well as gravity and surface tension are found to have a profound effect on both modes. For example, contrary to intuitive expectations, a specific choice of the interfacial surface tension proves to be a powerful destabilizing factor for the TS waves. An analysis of various limiting situations is presented in §§4 and 5. In §4 properties of short-wave instabilities are considered for $O(1)$ parameters of the two fluids. In §§4.2, 4.3 the TS-wave destabilization by surface tension is described analytically in terms of linear interaction between growing TS and decaying interfacial waves. In §4.4 the short-wave interfacial instability arising in the case of negligible surface tension and a less viscous fluid in the film is shown to be linked with the mode identified by Hooper & Boyd (1987). Section 5 is specifically devoted to flows with increased film viscosity. It is shown that viscous/inviscid interaction alters the known long-wave instability properties, the growth rate being

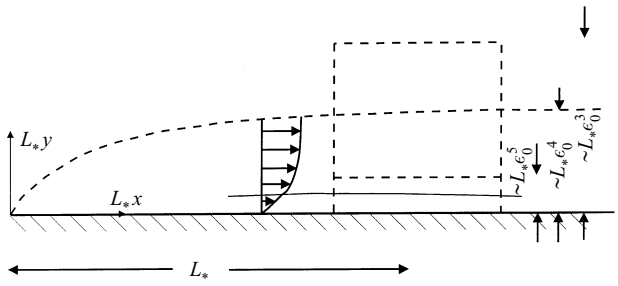

FIGURE 1. A sketch illustrating the unperturbed boundary layer and film in the asymptotic structure of the interaction region.

reduced from $O\left(k^2\right)$ in Yih (1967) and $O\left(k^{4/3}\right)$ in Hooper (1985) to $O\left(k^{8/3}\right)$ when the wavenumber k is small. Interfacial instability on very viscous films for $O(1)$ and increased wavenumbers is studied in §§5.2 and 5.3, respectively, whereas the effect of higher film viscosity on the TS waves is considered in §5.4. A discussion and comparisons with experimental observations by Ludwieg & Hornung (1989) are given in §6.

2. Derivation of the viscous/inviscid interaction equations

We consider laminar boundary-layer flow on a horizontal flat plate coated with a thin film of fluid different from and immiscible with the ambient fluid in the boundary layer; see figure 1. The Cartesian coordinates along and normal to the plate with the origin at the leading edge are denoted as L_*x, L_*y, the corresponding velocity components are U_*u, U_*v, and the time is $L_*U_*^{-1}t$, using the typical free-stream speed U_* and the development length of the boundary layer L_* as reference quantities. The variable part of the pressure function is $\rho_*U_*^2p^{\pm}$, ρ_* being the density of the main fluid. In what follows the sign convention is used to distinguish between the flow in the boundary layer (plus) and in the film (minus). The non-dimensional densities and kinematic viscosities of the two fluids referred to the corresponding dimensional parameters ρ_*, ν_* of the boundary layer are denoted as $\rho^{\pm}, \nu^{\pm}$.

The non-dimensional Navier–Stokes equations can be written in the form

$$\frac{\partial \boldsymbol{U}^{\pm}}{\partial t} + \left(\boldsymbol{U}^{\pm}\cdot\nabla\right)\boldsymbol{U}^{\pm} = -\frac{1}{\rho^{\pm}}\nabla p^{\pm} - \frac{\boldsymbol{j}}{Fr} + \frac{1}{Re}\nu^{\pm}\nabla^2\boldsymbol{U}^{\pm}, \quad \nabla\cdot\boldsymbol{U}^{\pm} = 0, \tag{2.1}$$

where $\boldsymbol{U}^{\pm} = \left(u^{\pm}, v^{\pm}\right)$ is the vector velocity, $\boldsymbol{j}$ denotes a unit vector in the vertical direction, and $Re = U_*L_*\nu_*^{-1}$, $Fr = U_*^2(g_*L_*)^{-1}$ are the Reynolds and the Froude numbers respectively, g_* being the gravitational acceleration.

The non-dimensionalization above implies that $\rho^+ = \nu^+ = 1$; however in the analysis in this section it is convenient to retain symbolic notation for the upper-fluid parameters.

As indicated in §1, the perturbed motion at a chosen x-station (in what follows at $x = 1$ without loss of generality) is assumed to have the streamwise and temporal scales of the same order of magnitude as the lower-branch TS instability. At large values of the Reynolds number these are

$$x - 1 = O\left(\varepsilon_0^3\right), \quad t = O\left(\varepsilon_0^2\right), \tag{2.2}$$

where $\varepsilon_0 = Re^{-1/8}$ is the main small parameter of a three-tier disturbance structure

which includes a viscous sublayer of thickness $y = O\left(\varepsilon_0^5\right)$, the bulk of the boundary layer with $y = O\left(\varepsilon_0^4\right)$, and the outer potential-flow zone $y = O\left(\varepsilon_0^3\right)$. The interface between two fluids passing through the lower tier can therefore be described by

$$y_{int} = \varepsilon_0^5 f\left(x, \frac{x-1}{\varepsilon_0^3}, \frac{t}{\varepsilon_0^2}\right) + \ldots, \tag{2.3}$$

keeping in mind that in the unperturbed state the fast x- and t-dependence vanishes, so that (2.3) reduces to $y_{int} = \varepsilon_0^5 f(x) + \ldots$.

At the interface the velocities and the tangential stress must be continuous, whereas the normal-stress condition in the current thin-film geometry simplifies to a pressure-jump discontinuity, namely

$$p^+ - p^- = \gamma \frac{\partial^2 y_{int}}{\partial x^2} \quad \text{at} \quad y = y_{int}, \tag{2.4}$$

with $\gamma = \gamma_* / \left(L_* \rho_* U_*^2\right)$ being a non-dimensional representation of the surface tension coefficient γ_*.

To introduce the appropriate scalings for the Froude number and for the surface tension coefficient, we notice that the pressure variation induced by local changes in the interface position is of order $\partial y_{int}/\partial x = O\left(\varepsilon_0^2\right)$. Then the pressure differences due to buoyancy forces, $\Delta p^{\pm} = O\left(y_{int}/Fr\right) = O\left(\varepsilon_0^5/Fr\right)$, and the pressure jump in (2.4) will both enter the triple-deck formulation provided that

$$Fr = \varepsilon_0^3 Fr_0, \quad \gamma = \varepsilon_0^3 \gamma_0, \tag{2.5}$$

with Fr_0 and γ_0 regarded as $O(1)$ parameters.

2.1. *The unperturbed boundary layer and film*

Since the main concern of this work is the properties of fully developed flows we ignore the details of how the film is produced. This will be a reasonable approximation at a certain distance from for example the front contact line of an oil patch on a plate, the approximation being better for thinner films. Then the steady boundary layer unaffected by instabilities can be treated as predominantly independent of the film flow; see e.g. Nelson *et al.* (1995). In the bulk of the boundary layer, where the vertical coordinate $y_1 = y\varepsilon_0^{-4}$ is of $O(1)$, the velocity components and pressure can be written in the form

$$u^+ = \hat{U}_0^+(x, y_1) + \varepsilon_0 \hat{U}_1^+(x, y_1) + O\left(\varepsilon_0^2\right), \tag{2.6}$$

$$v^+ = \varepsilon_0^4 \left[\hat{V}_0^+(x, y_1) + \varepsilon_0 \hat{V}_1^+(x, y_1) + O\left(\varepsilon_0^2\right)\right], \tag{2.7}$$

$$p^+ = \hat{P}_0^+(x) - \varepsilon_0 y_1 \rho^+ / Fr_0 + O\left(\varepsilon_0^4\right). \tag{2.8}$$

Here the main-order velocities $\hat{U}_0^+, \hat{V}_0^+$ represent the usual single-fluid boundary layer under a specified external pressure $\hat{P}_0^+(x)$. In the case of a uniform outer stream, for example, we have $\hat{P}_0^+ \equiv \text{const}$, so that the solution for $\hat{U}_0^+, \hat{V}_0^+$ can be expressed in terms of the Blasius streamfunction. The $O(\varepsilon_0)$ velocity corrections in (2.6), (2.7) are then governed by linearized boundary-layer equations without pressure forcing and also with the trivial outer-edge condition $\hat{U}_1^+ \to 0$ as $y_1 \to \infty$, but with a non-vanishing slip velocity at the wall, $\hat{U}_1^+(x, 0) = \hat{U}_s(x)$ say. The slip effect is due to the presence of the film where the flow is driven by the shear stress in the lower part of

the main boundary layer. In the film we define $Y = y\varepsilon_0^{-5}$ to be of $O(1)$ and expand the flow functions in the form

$$u^- = \varepsilon_0 \hat{U}_0^-(x, Y) + O\left(\varepsilon_0^2\right), \quad v^- = \varepsilon_0^6 \hat{V}_0^-(x, Y) + O\left(\varepsilon_0^7\right), \tag{2.9}$$

$$p^- = \hat{P}_0^+(x) + O\left(\varepsilon_0^2\right), \tag{2.10}$$

with the immediate result

$$\hat{U}_0^- = \hat{\lambda}^+(x)\, Y \rho^+ v^+ / \left(\rho^- v^-\right), \quad \hat{V}_0^- = -\tfrac{1}{2}[\hat{\lambda}^+(x)]' Y^2 \rho^+ v^+ / \left(\rho^- v^-\right), \tag{2.11}$$

for the main-order velocities. Here $\hat{\lambda}^+(x) = \partial \hat{U}_0^+ / \partial y_1 \,(y_1 = 0)$ is the wall shear in the boundary layer, and the prime designates the derivative. The solution (2.11) satisfies the tangential-stress continuity at the interface at $Y = f(x)$. The continuity of the streamwise velocity then yields

$$\hat{U}_s(x) = \hat{\lambda}^+ f\left[1 - \rho^+ v^+ / \left(\rho^- v^-\right)\right], \tag{2.12}$$

with the shape of the interface $f(x)$ determined by $\hat{\lambda}^+ f^2 = \text{const}$, as follows from the mass conservation within the film; cf. Nelson *et al.* (1995).

2.2. *Equations of viscous/inviscid interaction*

For the flow within the interaction region shown in figure 1 the appropriate local variables are the shorter-scale coordinate $X = (x - 1)\varepsilon_0^{-3}$ and the fast time $T = t\varepsilon_0^{-2}$, with X and T of $O(1)$, so that the interface position is written as $y_{int} = \varepsilon_0^5 F(X, T) + \ldots$, cf. (2.3). In the main part of the boundary layer, $y_1 = O(1)$, the perturbed-flow expansions of the form

$$u^+ = U_{00}(y_1) + \varepsilon_0 \left[A(X, T)\, U_{00}' + U_{01}(y_1)\right] + \ldots, \quad v^+ = \varepsilon_0^2 \left[-\frac{\partial A}{\partial X} U_{00}\right] + \ldots, \tag{2.13}$$

$$p^+ = P_{00} - \varepsilon_0 y_1 \rho^+ / Fr_0 + \varepsilon_0^2 P^+(X, T) + \ldots, \tag{2.14}$$

hold, similar to the usual triple-deck solution but with the extra contribution U_{01} in the horizontal velocity and, more significantly for buoyant fluids, with the vertical pressure variation of order ε_0. The unknown displacement function A and the pressure term P^+ are linked via the standard principal-value integral,

$$P^+ = \rho^+ [U_{00}(\infty)]^2 \frac{1}{\pi} \int_{-\infty}^{\infty} \frac{\partial A(s, T)}{\partial s} \frac{\mathrm{d}s}{X - s}, \tag{2.15}$$

as follows from the potential-flow requirements in the uppermost part of the interaction region. The pressure constant P_{00} and the velocity terms U_{00}, U_{01} in (2.13), (2.14) are determined in principle by the flow upstream, in particular $U_{00} = \hat{U}_0^+(1, y_1)$, $U_{01} = \hat{U}_1^+(1, y_1)$, $P_{00} = \hat{P}_0^+(1)$. The crucial viscous effects are accumulated in a thin near-wall zone where

$$u^\pm = \varepsilon_0 U^\pm(X, Y, T) + \ldots, \quad v^\pm = \varepsilon_0^3 V^\pm(X, Y, T) + \ldots, \tag{2.16}$$

$$p^\pm = P_{00} + \varepsilon_0^2 \left[-Y \rho^\pm / Fr_0 + P^\pm(X, T)\right] + \ldots \quad \text{with} \quad Y = \varepsilon_0^{-5} y = O(1). \tag{2.17}$$

On substituting into (2.1), the leading terms here are governed by the equations,

$$\frac{\partial U^\pm}{\partial T} + U^\pm \frac{\partial U^\pm}{\partial X} + V^\pm \frac{\partial U^\pm}{\partial Y} = -\frac{1}{\rho^\pm} \frac{\partial P^\pm}{\partial X} + v^\pm \frac{\partial^2 U^\pm}{\partial Y^2}, \tag{2.18}$$

$$\frac{\partial U^{\pm}}{\partial X}+\frac{\partial V^{\pm}}{\partial Y}=0. \tag{2.19}$$

The flow in the film must satisfy the no-penetration and no-slip conditions,

$$U^{-}=V^{-}=0 \quad \text{at} \quad Y=0, \tag{2.20}$$

whereas the match with the potential-flow zone across the main part of the boundary layer provides the conditions for the flow above the interface, namely

$$U^{+}=\lambda^{+}(Y+A)+U_s+o(1), \quad V^{+}=-\lambda^{+}Y\frac{\partial A}{\partial X}+O(1) \quad \text{as} \quad Y\to\infty, \tag{2.21}$$

where U_s is a constant, $U_s=\hat{U}_s(1)=U_{01}(0)$, see (2.12), (2.13). The remaining boundary conditions are formulated as the velocity and tangential-stress continuity at the interface,

$$U^{+}=U^{-}, \quad V^{+}=V^{-}=\frac{\partial F}{\partial T}+U^{\pm}\frac{\partial F}{\partial X}, \tag{2.22}$$

$$\rho^{+}\nu^{+}\frac{\partial U^{+}}{\partial Y}=\rho^{-}\nu^{-}\frac{\partial U^{-}}{\partial Y} \quad \text{at} \quad Y=F(X,T), \tag{2.23}$$

with the interfacial kinematic condition also included in (2.22). The unperturbed-flow velocities are given by

$$U^{+}=\lambda^{+}Y+U_s \quad \text{if} \quad Y>a, \quad U^{-}=\lambda^{-}Y \quad \text{if} \quad 0<Y<a, \quad V^{\pm}=0, \tag{2.24}$$

where $a=f(1)=\text{const}$ is the scaled local film thickness in the base flow, and $\lambda^{+}=\hat{\lambda}^{+}(1), \lambda^{-}=\lambda^{+}\rho^{+}\nu^{+}/(\rho^{-}\nu^{-})$, see (2.11). The pressure-displacement relation (2.15) together with the pressure jump,

$$P^{+}-P^{-}=\gamma_0\frac{\partial^2 F}{\partial X^2}+\frac{\rho^{+}-\rho^{-}}{Fr_0}F, \tag{2.25}$$

complete the boundary-value formulation for the flow in the interaction region.

The change of variables,

$$\left[X,Y,T,U^{\pm},V^{\pm},P^{\pm},a,F,\gamma_0,Fr_0\right]\to\left[\alpha^3\lambda^{+}X,\alpha Y,\alpha^2 T,\alpha\lambda^{+}U^{\pm},\alpha^{-1}V^{\pm},\right.$$

$$\left.\alpha^2\left(\lambda^{+}\right)^2P^{\pm},\alpha a,\alpha F,\alpha^7\left(\lambda^{+}\right)^4\gamma_0,\alpha^{-1}\left(\lambda^{+}\right)^{-2}Fr_0\right], \tag{2.26}$$

with $\alpha=[U_{00}(\infty)]^{1/2}\left(\lambda^{+}\right)^{-3/4}$ indicates that two parameters, $U_{00}(\infty)$ and λ^{+}, can be taken equal to unity without loss of generality. We also recall that $\rho^{+}=\nu^{+}=1$ according to the non-dimensionalization. Hence the interaction formulation is left with five scaled parameters: the viscosity and density of the film fluid ρ^{-} and ν^{-}, the initial film thickness a, and the surface tension and gravity constants γ_0 and Fr_0. In the following sections we consider a linearized version of the problem.

3. Linear stability problem

Disturbances to the basic-state flow (2.24) with a small typical amplitude $\delta\ll 1$ are taken in the normal-mode form,

$$U^{\pm}=u_{00}+\lambda^{\pm}\bar{Y}+\delta E\bar{u}^{\pm}\left(\bar{Y}\right)+\ldots, \quad V^{\pm}=\delta E\bar{v}^{\pm}\left(\bar{Y}\right)+\ldots, \tag{3.1}$$

$$\left[P^{\pm},F,A\right]=[0,a,0]+\delta E\left[\bar{p}^{\pm},\bar{f},\bar{A}\right]+\ldots, \tag{3.2}$$

where $E = \exp[\mathrm{i}(kX - \omega T)]$, the wavenumber k is real, the frequency $\omega = \omega_r + \mathrm{i}\omega_i$ is in general complex, and the disturbance is said to be unstable if the imaginary part ω_i is positive. The new vertical coordinate $\bar{Y} = Y - a$ measured from the unperturbed interface is introduced for convenience, so that the boundary-layer part of the flow and the film occupy the regions $\bar{Y} \geqslant 0$ and $-a \leqslant \bar{Y} \leqslant 0$ in turn. Also $u_{00} = a\lambda^-$ is the basic-state interfacial velocity.

On substituting (3.1), (3.2) into (2.15), (2.18)–(2.25) and taking $U_{00}(\infty) = \lambda^+ = \rho^+ = v^+ = 1$, the governing formulation acquires the form

$$\mathrm{i}\left(k\bar{Y} + ku_{00} - \omega\right)\bar{u}^+ + \bar{v}^+ = -\mathrm{i}k\bar{p}^+ + \bar{u}^{+\prime\prime}, \quad \mathrm{i}k\bar{u}^+ + \bar{v}^{+\prime} = 0, \tag{3.3}$$

$$\bar{u}^+(\infty) = \bar{A}, \quad \bar{p}^+ = |k|\bar{A}, \tag{3.4}$$

$$\mathrm{i}\left(k\lambda^-\bar{Y} + ku_{00} - \omega\right)\bar{u}^- + \lambda^-\bar{v}^- = -\frac{\mathrm{i}k}{\rho^-}\bar{p}^- + v^-\bar{u}^{-\prime\prime}, \quad \mathrm{i}k\bar{u}^- + \bar{v}^{-\prime} = 0, \tag{3.5}$$

$$\bar{u}^-(-a) = \bar{v}^-(-a) = 0, \tag{3.6}$$

$$\bar{p}^+ - \bar{p}^- = -\left[\gamma_0 k^2 + \frac{\rho^- - 1}{Fr_0}\right]\bar{f}, \quad \bar{v}^{\pm}(0) = \mathrm{i}(ku_{00} - \omega)\bar{f}, \tag{3.7}$$

$$\left(1 - \lambda^-\right)\bar{f} + \bar{u}^+(0) - \bar{u}^-(0) = 0, \quad \bar{u}^{+\prime}(0) = \rho^- v^- \bar{u}^{-\prime}(0). \tag{3.8}$$

The relations (3.3)–(3.8) form an eigenvalue problem for the disturbance frequency in terms of the wavenumber and the parameters $\gamma_0, Fr_0, a, \rho^-, v^-$. The interfacial velocity and the shear in the film can be expressed through the other parameters as $u_{00} = a\lambda^-$ and $\lambda^- = 1/(\rho^- v^-)$, respectively.

3.1. *Numerical solutions of the eigenvalue problem*

Computational solutions of (3.3)–(3.8) were obtained with the use of a numerical method described in the Appendix. For ease of reference the results are divided into three groups.

(i) *Equal densities, no surface tension.* If $\gamma_0 = 0, \rho^- = 1$ and the unperturbed film thickness is fixed ($a = 1$ for the solutions illustrated below), then in addition to the variable wavenumber the only free parameter is the kinematic viscosity of the lower fluid v^- or, equivalently, the shear $\lambda^- = 1/v^-$. Such an artificial flow model provides a good starting example for identifying the key instabilities associated with the TS mechanism and with the presence of the interface, cf. Yih (1967), Hooper & Boyd (1983, 1987).

Figure 2(*a,b*) illustrates the effect of film viscosity on the TS instability which is characterized conventionally by a finite-limit growth rate, $\omega_i = O(1)$, and linearly increasing phase speed, $c_r (= \omega_r/k) = O(|k|)$ for short waves with $k \gg 1$. The solution with $\lambda^- = 1$ (corresponding to a homogeneous fluid) has the limit properties $\omega_i = 1/\sqrt{2} + \ldots, c_r = |k| + \ldots$, as $k \to \infty$, see e.g. Ryzhov & Terent'ev (1986) and Smith (1986). Increased viscosity of the film fluid ($v^- > 1, \lambda^- < 1$) results in stronger instability for shorter waves. The trends in figure 2(*a*) suggest that the constant in the limit growth rate as $k \to \infty$ varies with v^- monotonically, with larger limit values for more viscous films. For a fixed wavenumber k, however, the complex frequency of a TS-type disturbance rolling over an extremely viscous film proves to be exactly the same as in the flow without a viscosity difference, see figure 2(*c*). The last property is not entirely unexpected, for the interfacial conditions in (3.7), (3.8) show that $\bar{u}^-, \bar{v}^-$ and $\bar{p}^-$, together with λ^-, are all quantities of order $1/v^-$ when $v^- \to \infty$, hence in the limit $v^- \to \infty, k = O(1)$ the disturbance frequency is determined by (3.3), (3.4)

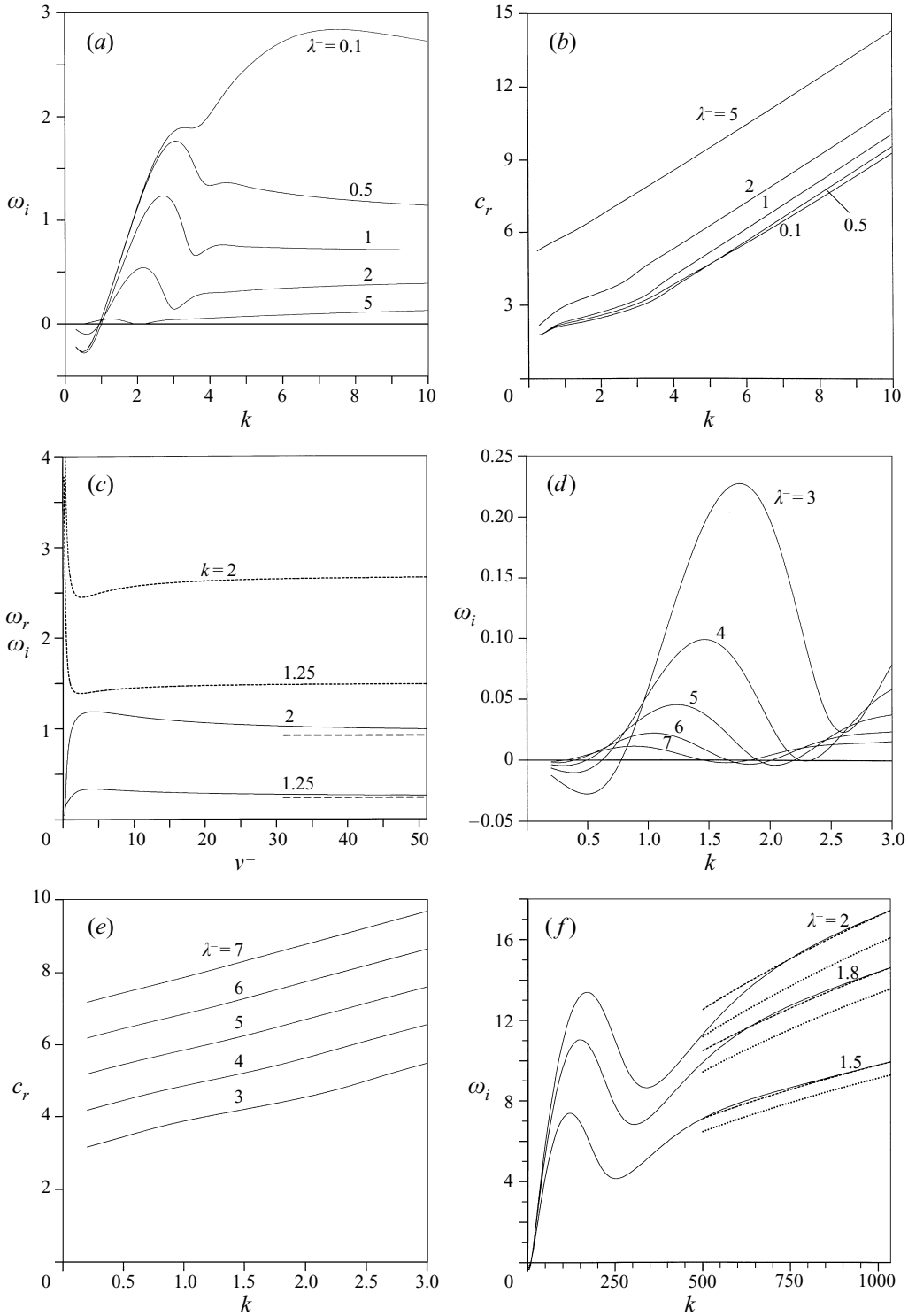

FIGURE 2 (*a–f*). For caption see facing page.

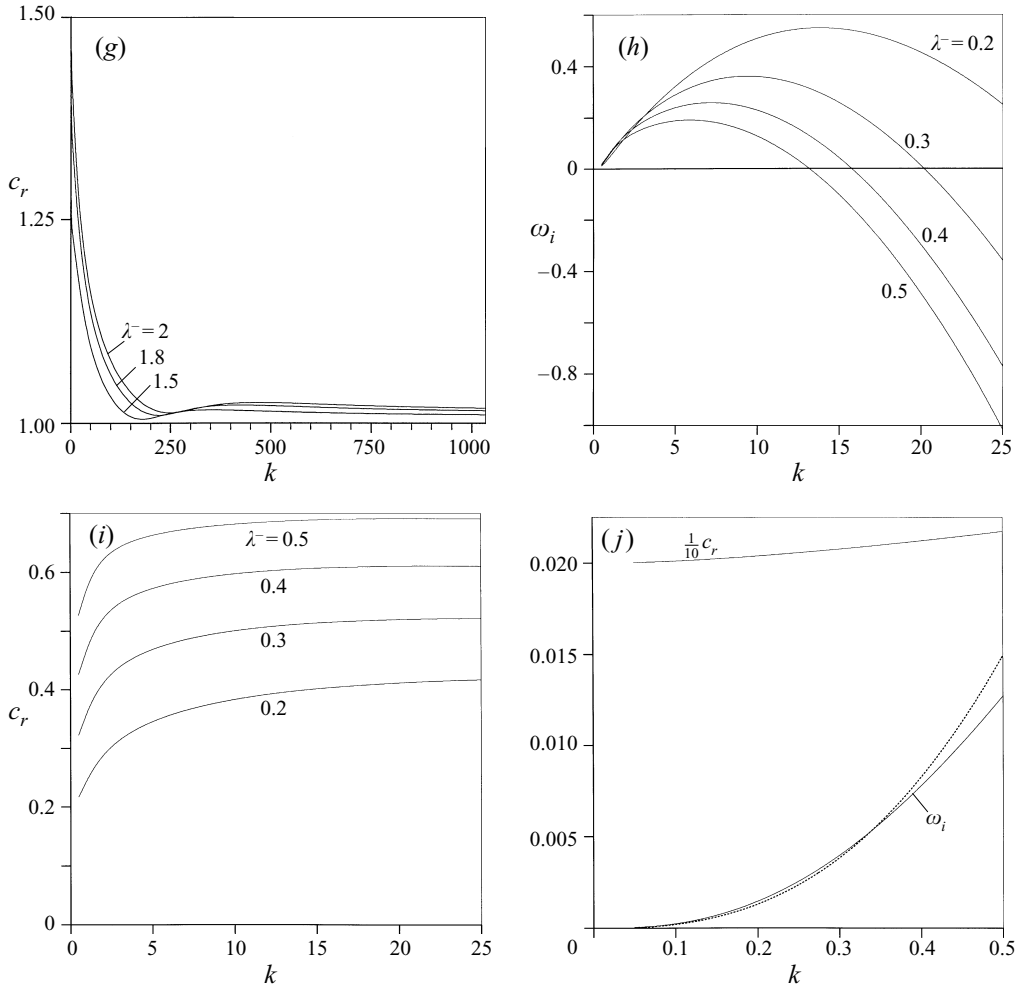

FIGURE 2. Numerical solutions of (3.3)–(3.8) for the TS and interfacial modes in the case of fluids of equal density and without surface tension, $\rho^- = 1, Fr_0 = \infty, \gamma_0 = 0$, and with $a = 1$. (a, b) The growth rate ω_i and the real part of the phase speed c_r of the TS instability versus k for variable $\lambda^- = 1/\nu^-$; (c) ω_i (solid) and ω_r (dotted) versus ν^- for two selected wavenumbers $k = 1.25$ and $k = 2$, the horizontal dashed lines show the corresponding growth rates at $\nu^- = 1$; (d, e) ω_i and c_r of the TS waves versus k for small wavenumbers and decreased film viscosity; (f, g) ω_i and c_r versus k for the short-wave interfacial mode in the case of smaller film viscosity, the dots show the asymptote (4.46) and the dashes the same asymptote but shifted up by a constant; (h, i) ω_i and c_r versus k for the long-wave interfacial mode in the flow with more viscous film fluid; (j) the long-wave limit behaviour of the interfacial mode in the case $\lambda^- = 0.2$. The dots show the asymptotic growth rates (5.8).

with the constraints $\bar{u}^+(0) = \bar{v}^+(0) = 0$ at the effectively 'solid' interface at $y = 0$. The diverse behaviour of the limit solutions when $\nu^- \to \infty$ for $k = O(1)$ and when $k \to \infty$ for an $O(1)$ viscosity ν^- indicates that faster growing instability develops at increased wavenumbers when the film is very viscous, see for example the curve marked $\lambda^- = 0.1$ in figure 2(a). We discuss this property in more detail in §5.4.

In the case of smaller film viscosity ($\nu^- < 1, \lambda^- > 1$) the TS waves are strongly inhibited, the local maximum in $\omega_i(k)$ becomes smaller and tends to appear at lower

wavenumbers, whereas the most unstable modes occur as $k \to \infty$. A peculiar feature illustrated more clearly in figure 2(*d,e*) is a complete stabilization in a part of the TS spectrum by a sufficiently low-viscosity film, when $\lambda^- \gtrsim 4$, or $\nu^- \lesssim 0.25$. The phase speed c_r of the 'detached' unstable mode at smaller k is an almost linear function of the wavenumber, see figure 2(*e*), which indicates a predominantly inviscid character of the disturbances.

Along with the TS modes associated primarily with the shearing motion in the main boundary layer the flow is also subject to interfacial instabilities. Figure 2(*f,g*) illustrates the interfacial mode for a less viscous fluid in the film. An analysis in §4.4 below shows that this short-wave mode which has no global maximum of the growth rate in the current regime (unless surface tension is included, see later in this section) is related to the instability described in Hooper & Boyd (1987). A graphical comparison with the short-wave asymptote is made in figure 2(*f*). The approach to the square-root limiting form given by (4.46) of §4.4 is seen to be slow, probably on account of the local growth-rate maximum occupying a considerable portion of the spectrum, and a better agreement with the asymptotic solution can be achieved by including an $O(1)$ correction term, as also shown in the figure. A similar maximum was also noted for some other combinations of the film parameters; the results for other cases will be presented in a separate paper. The flow regime at hand provides the lower neutral branch for such waves and therefore may prove significant for the wave formation in a non-parallel spatially-developing flow (by analogy with the TS instability in boundary layers); however the major events involving this kind of instability are likely to be concentrated in the range of much shorter disturbances (again if surface tension is negligibly small).

When the film viscosity exceeds the viscosity of the main current the interfacial mode arises in a long-wave range, see figure 2(*h,i*), although the growth rate maximum and the unstable k-range both gradually increase for greater values of ν^-. For this mode the present theory predicts the position of the upper neutral branch. A close-up in figure 2(*j*) of a small-k interval for one such solution leaves little doubt that the instability persists for arbitrarily long waves (within the triple-deck scaling), with the phase speed approaching the interfacial velocity from above, $c_r \to u_{00}+$, and $\omega_i \to 0$ in the limit when $k \to 0$ (note that $u_{00} = a\lambda^- = 0.2$ for the case illustrated in the figure).

(ii) *Unequal densities in stable stratification, no surface tension.* Even at infinitely large Froude numbers the interfacial density difference may have a considerable impact on the instability properties by altering the dynamic viscosity of the film fluid and changing the convection/pressure balance in the momentum equations. It seems more appropriate, however, to examine the density effects in conjunction with gravity. Numerical solutions in figure 3(*a,b*) illustrate the effect of increased gravity on the TS instability. The density and viscosity of the film are fixed at moderate values $\nu^- = \rho^- = 2$. As the Froude number decreases the growth rate maximum is shifted towards larger k; however extremely short waves remain mostly unaffected by gravity. The dependence of the real phase speed on the Froude number is less pronounced, see figure 3(*b*).

If, alternatively, the Froude number and kinematic viscosity of the film are kept constant and the density of the lower fluid increases, the growth-rate diagram tends to return to the single-fluid solution, see figure 3(*c*), obviously due to the 'solidification' of the interface similar to the effect of high film viscosity in the previous item.

The effect of the Froude number and density variations on interfacial waves will be examined analytically in a subsequent section.

(iii) *The effect of surface tension.* Surface tension has a strong, non-monotonic, and at first sight a rather unexpected effect on the TS instability, especially in the

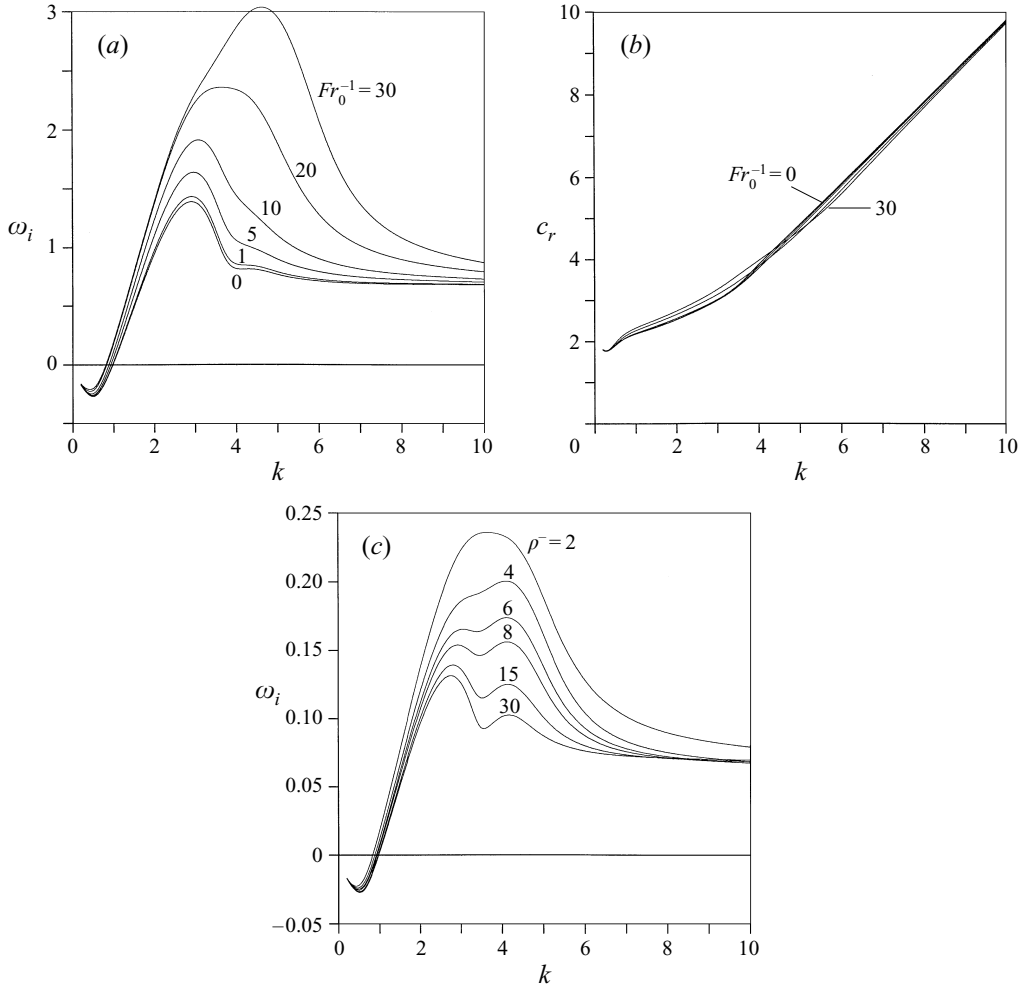

FIGURE 3. The effect of the Froude number and density variation on the TS instability. (*a*, *b*) ω_i and c_r versus k for the flow with $\nu^- = \rho^- = 2, a = 1, \gamma_0 = 0$; (*c*) ω_i versus k for varying ρ^-, the other parameters are $a = 1, \nu^- = 2, Fr_0^{-1} = 20, \gamma_0 = 0$.

short-wave range (the influence on longer waves is weak for obvious reasons), see figure 4(*a,b*). Contrary to the commonly observed short-wave stabilization (as, for instance, in the case of Kelvin–Helmholtz modes) short TS waves with large k prove to be less stable when surface tension is included. For the flow illustrated in figure 4(*a,b*) the asymptotic growth-rate at large wavenumbers grows monotonically when γ_0 increases from 0 to a critical value $\gamma_0 = \gamma_c$ (= 2 in this particular example). At the critical value $\gamma_0 = \gamma_c$ the growth rate of short waves becomes unbounded. However at supercritical values $\gamma_0 > \gamma_c$ the growth-rate distribution returns to its usual shape with a finite plateau at infinity. The behaviour of the real part of the phase speed in figure 4(*b*) indicates the asymptote, $c_r = k + \ldots$, at large positive k regardless of surface tension, although the correction to the first linear term seems to have a non-monotonic dependence on γ_0. An asymptotic solution developed below in §4.3 indicates that at the critical value $\gamma_0 = 2$ the limiting growth rate is given by $\omega = 2k^{3/2} + O(k)$, when $k \to \infty$. A comparison with this result is shown in figure 4(*c*).

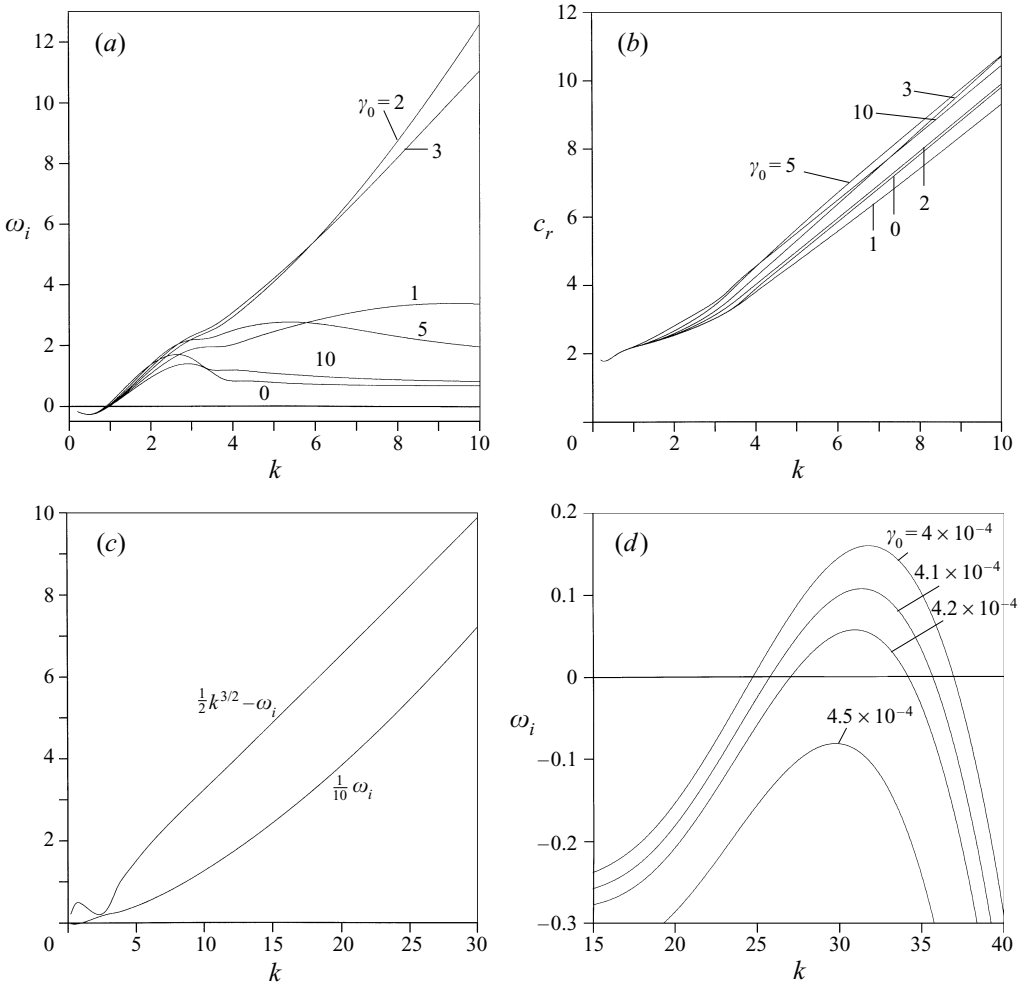

FIGURE 4. The effect of surface tension. (*a*, *b*) ω_i and c_r versus k for the TS mode and $v^- = \rho^- = 2, a = 1, Fr_0^{-1} = 0$; (*c*) a plot of $\frac{1}{10}\omega_i$ and of $\frac{1}{2}k^{3/2} - \omega_i$ versus k in the same regime with $\gamma_0 = 2$ shown for comparison with (4.38); (*d*) ω_i versus k for the short-wave interfacial instability, the flow with $\rho^- = 1, v^- = 0.5, a = 1$.

A short-wave interfacial instability arises when the film is less viscous than the main fluid, as discussed earlier in this section. Surface tension has a powerful stabilizing influence on such waves, see figure 4(*d*). The effect of surface tension on long-wave instability in more viscous films will be discussed in §5.

4. Asymptotic properties of short-wave instabilities

In this section the eigenvalue problem (3.3)–(3.8) is solved analytically for large values of the disturbance wavenumber k.

4.1. *Short-wave TS instability*

Consider first the TS instability with large wavenumbers. To begin with, all the flow parameters (except k) in the starting formulation are assumed to be of $O(1)$, and the

disturbance wavenumber and frequency are taken in the form

$$k = \varepsilon^{-1}k_0, \quad \omega = \varepsilon^{-2}\omega_0 + \varepsilon^{-1}\omega_1 + \omega_2 + \ldots, \tag{4.1}$$

where ε is an artificial small parameter and $k_0 = O(1)$. The shortened streamwise length scale implies a predominantly inviscid perturbed motion except in thin near-wall and interfacial viscous layers. In the flow above the interface the appropriate variable is $\tilde{Y} = \varepsilon\bar{Y} = O(1)$, and then the flow functions expand in the form

$$\left[\bar{u}^+, \bar{A}\right] = \left[u_0^+, A_0\right] + \varepsilon\left[u_1^+, A_1\right] + \varepsilon^2\left[u_2^+, A_2\right] + \ldots, \tag{4.2}$$

$$\bar{v}^+ = \varepsilon^{-2}v_0^+ + \varepsilon^{-1}v_1^+ + v_2^+ + \ldots, \quad \bar{p}^+ = \varepsilon^{-1}p_0^+ + p_1^+ + \varepsilon p_2^+ + \ldots, \tag{4.3}$$

where, to satisfy the governing equations and the conditions at infinity, we take

$$u_0^+ = A_0, \quad v_0^+ = -\mathrm{i}k_0A_0\tilde{Y}, \quad p_0^+ = |k_0|A_0, \tag{4.4}$$

$$u_1^+ = A_1, \quad v_1^+ = -\mathrm{i}k_0A_1\tilde{Y} - \mathrm{i}\left(k_0u_{00} - \omega_1\right)A_0, \quad p_1^+ = |k_0|A_1, \tag{4.5}$$

$$u_2^+ = A_2, \quad v_2^+ = -\mathrm{i}k_0A_2\tilde{Y} + \mathrm{i}\omega_2A_0 - \mathrm{i}\left(k_0u_{00} - \omega_1\right)A_1, \quad p_2^+ = |k_0|A. \tag{4.6}$$

The main-order momentum balance also provides the leading disturbance frequency,

$$\omega_0 = k_0|k_0|. \tag{4.7}$$

In the film ($-a < \bar{Y} < 0, \bar{Y} \sim 1$) we have

$$\left.\begin{gathered}\left[\bar{u}^-, \bar{v}^-\right] = \left[u_0^-, \varepsilon^{-1}v_0^-\right] + \left[\varepsilon u_1^-, v_1^-\right] + \ldots, \\ u_0^- = \frac{k_0}{\omega_0\rho^-}p_0^-, \quad u_1^- = \frac{k_0}{\omega_0\rho^-}\left[p_1^- - \frac{\omega_1}{\omega_0}p_0^-\right], \quad v_0^- = -\frac{\mathrm{i}k_0^2}{\omega_0\rho^-}\left(\bar{Y} + a\right)p_0^-, \\ v_1^- = -\frac{\mathrm{i}k_0^2}{\omega_0\rho^-}\left(\bar{Y} + a\right)\left[p_1^- - \frac{\omega_1}{\omega_0}p_0^-\right] + v_w,\end{gathered}\right\} \tag{4.8}$$

$$\bar{f} = \varepsilon f_1 + \varepsilon f_2 + \ldots, \quad \bar{p}^- = \varepsilon^{-1}p_0^- + p_1^- + \ldots, \tag{4.9}$$

where the velocity components have been expressed in terms of the pressure contributions, and the constant of integration v_w is included on account of the near-wall viscous (Stokes) layer. The conventional oscillatory-flow result for the latter can be written as

$$v_w = \mathrm{i}k_0^2p_0^-\left(\omega_0\rho^-\varkappa^-\right)^{-1}, \quad \text{where} \quad \varkappa^- = \left(-\mathrm{i}\omega_0/\nu^-\right)^{1/2}, \quad |\arg\varkappa^-| < \pi/2. \tag{4.10}$$

In a single-fluid flow the Stokes displacement v_w provides the key instability mechanism for short TS waves away from the lower neutral branch. In the two-fluid flow an additional displacement of a comparable order of magnitude is produced also in viscous layers on both sides of the interface, where $\bar{Y} = \varepsilon\eta$ and η is of $O(1)$. For the leading terms in the interfacial layers we have

$$\bar{u}^\pm = \tilde{U}_0^\pm(\eta) + \ldots, \quad \bar{v}^\pm = \varepsilon^{-1}v_0^-(0) + \tilde{V}_0^\pm(\eta) + \ldots, \quad \bar{p}^\pm = \varepsilon^{-1}p_0^\pm + \ldots, \tag{4.11}$$

$$\tilde{U}_0^\pm = \frac{k_0p_0^\pm}{\omega_0\rho^\pm}\left[1 - \exp\left(\mp\varkappa^\pm\eta\right)\right] + D\exp\left(\mp\varkappa^\pm\eta\right), \tag{4.12}$$

$$\tilde{V}_0^\pm = -\frac{\mathrm{i}k_0^2p_0^\pm}{\omega_0\rho^\pm}\left[\eta \mp \frac{1}{\varkappa^\pm}\left(1 - \exp\left(\mp\varkappa^\pm\eta\right)\right)\right] \pm \frac{\mathrm{i}k_0}{\varkappa^\pm}D\left(\exp\left(\mp\varkappa^\pm\eta\right) - 1\right) + D_1, \tag{4.13}$$

with $\varkappa^{\pm} = \left(-\mathrm{i}\omega_0/v^{\pm}\right)^{1/2}, |\arg\left(\varkappa^{\pm}\right)| < \pi/2$, and

$$D = k_0\omega_0^{-1}\left(v^+\varkappa^+p_0^+ + v^-\varkappa^-p_0^-\right)\left(v^+\varkappa^+\rho^+ + v^-\varkappa^-\rho^-\right)^{-1}. \tag{4.14}$$

The parameters ρ^+, v^+ retained here for convenience will be set equal to unity in the final relations.

Matching the effectively inviscid-flow solutions (4.2), (4.3) and (4.8), (4.9) across the interfacial layers and the use of the kinematic and pressure-jump conditions allows us to express the shape corrections in (4.9) as well as the film-flow pressure terms p_0^-, p_1^- and the constant of integration D_1 in (4.13) in terms of the upper-flow displacement A_0. In addition, the frequency corrections are determined from the problem solvability in the successive approximations. So, omitting further details, the first frequency term ω_1 is found to be purely real,

$$\omega_1 = k_0u_{00} - ak_0\left(\rho^- - \gamma_0a\right)^{-1}, \tag{4.15}$$

whereas the disturbance growth rate $\omega_{2i} = \mathrm{Im}\,(\omega_2)$ can be written in the form

$$\omega_{2i} = \frac{1}{\sqrt{2}}\left(1 + \frac{\gamma_0a}{\rho^-S}\right)\left[1 + 2\frac{(v^-)^{1/2}}{S\rho^-} - \left(1 + \left(v^-\right)^{1/2}\right)\frac{1 + S^{-1}(v^-)^{1/2}}{1 + \rho^-(v^-)^{1/2}}\right]$$

$$- \frac{1}{\sqrt{2}}\frac{\gamma_0a}{\rho^-S}\left(1 - \frac{1 + S^{-1}(v^-)^{1/2}}{1 + \rho^-(v^-)^{1/2}}\right) \quad \text{with} \quad S = 1 - \frac{\gamma_0a}{\rho^-}. \tag{4.16}$$

This formula simplifies considerably if surface tension can be neglected (either because $\gamma_0 = 0$, or if the film is very thin, $a \ll 1$). Then

$$\omega_{2i} = \frac{1}{\sqrt{2}}\frac{\left[1 + (\rho^- - 1)^2\right](v^-)^{1/2} + \rho^-v^-}{\rho^-\left(1 + \rho^-(v^-)^{1/2}\right)}. \tag{4.17}$$

The right-hand side of (4.17) is always positive, hence instability persists for any combination of the film viscosity and density. Stronger instability is obtained if ρ^- is small, for then $\omega_{2i} = (2v^-)^{1/2}/\rho^- + \ldots$ as $\rho^- \to 0$, or if v^- is large, because $\omega_{2i} = (v^-)^{1/2}/\left(\rho^-\sqrt{2}\right) + \ldots$ as $v^- \to \infty$. The presence of a very dense fluid in the film results in effective solidification of the interface for these disturbances, hence $\omega_{2i} = 1/\sqrt{2} + \ldots$ as $\rho^- \to \infty$, whereas a very small film viscosity tends to suppress short TS waves, $\omega_{2i} \to 0$ as $v^- \to 0$. These trends are illustrated further in figure 5(*a*).

Surface tension changes the growth rates dramatically, as can be seen, for instance, in a somewhat exotic case of two fluids with equal density and viscosity, $\rho^- = v^- = 1$, when (4.16) reduces to

$$\omega_{2i} = 2^{-3/2}\left(2 + \gamma_0^2a^2\right)(1 - \gamma_0a)^{-2}. \tag{4.18}$$

Here the growth rate becomes infinite if $\gamma_0 = a^{-1}$. In the more general case given by (4.16) the unbounded growth rate appears if $S = 0$, that is when the surface tension coefficient reaches the critical value $\gamma_0 = \gamma_c = \rho^-/a$, as shown in figure 5(*b*). This is in agreement with the critical value $\gamma_c = 2$ encountered in the numerical solution in §3 for $\rho^- = 2, a = 1$ (see figure 4*a*). The origin of this singularity will become clearer when we examine the properties of capillary waves with large wavenumbers.

4.2. *Short capillary waves*

Capillary waves feature increased oscillations in the film compared with the disturbance in the main boundary layer. With the same frequency expansion (4.1) as in

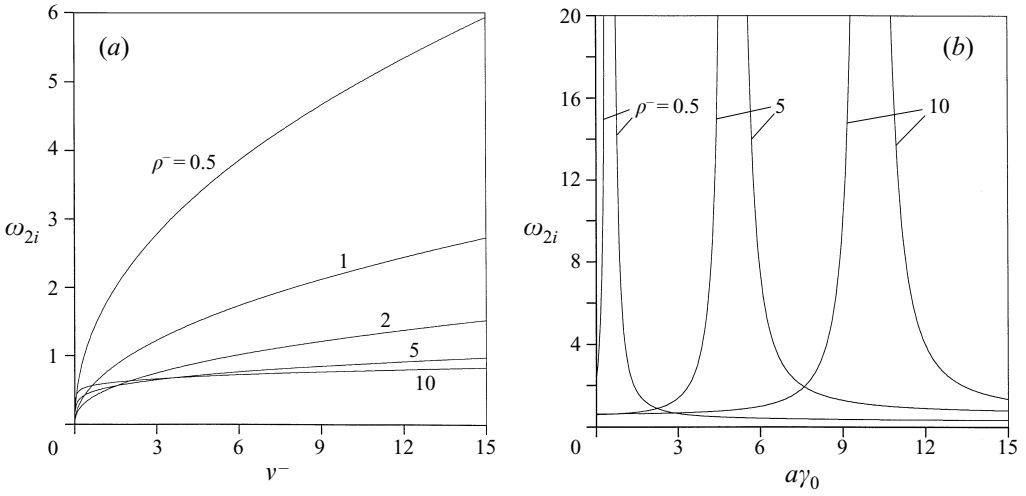

FIGURE 5. The limiting growth rate (4.16) of short TS waves. (*a*) ω_{2i} versus v^- for various ρ^- and $\gamma_0 = 0$; (*b*) ω_{2i} versus $a\gamma_0$ for various ρ^- and $v^- = 2$.

§4.1, the flow functions in the film are now given by

$$\bar{u}^- = \varepsilon^{-1}u_0^- + u_1^- + \ldots, \quad \bar{v}^- = \varepsilon^{-2}v_0^- + \varepsilon^{-1}v_1^- + \ldots, \tag{4.19}$$

$$\bar{p}^- = \varepsilon^{-2}p_0^- + \varepsilon^{-1}p_1^- + \ldots, \quad \bar{f} = f_0 + \varepsilon f_1 + \ldots, \tag{4.20}$$

where for the velocity terms shown explicitly the respective coefficients in (4.8) can be used. In the upper fluid the layer of thickness $O\left(\varepsilon^{-1}\right)$ is important again, with the same expansions (4.2), (4.3) but with a somewhat different solution,

$$u_0^+ = A_0, \quad v_0^+ = -\mathrm{i}k_0\tilde{Y}A_0 + \mathrm{i}\left(\omega_0 - k_0|k_0|\right)A_0, \quad p_0^+ = |k_0|A_0, \tag{4.21}$$

$$u_1^+ = A_1, \quad v_1^+ = -\mathrm{i}k_0\tilde{Y}A_1 + \mathrm{i}\left(\omega_0 - k_0|k_0|\right)A_1 + \mathrm{i}\left(\omega_1 - k_0u_{00}\right)A_0, \quad p_1^+ = |k_0|A_1. \tag{4.22}$$

In the interfacial viscous layer ($\bar{Y} = \varepsilon\eta, \eta = O(1)$) we obtain

$$\bar{u}^\pm = \varepsilon^{-1}\tilde{U}_0^\pm(\eta) + \ldots, \quad \bar{v}^\pm = \varepsilon^{-2}v_0^-(0) + \varepsilon^{-1}\tilde{V}_0^\pm(\eta) + \ldots, \tag{4.23}$$

$$\tilde{V}_0^+ = \frac{\mathrm{i}k_0^2p_0^-}{\varkappa^+\rho^-\omega_0}\frac{\rho^-(v^-)^{1/2}}{1+\rho^-(v^-)^{1/2}}\exp\left(-\varkappa^+\eta\right) + D^+, \quad D^+ = \text{const}, \tag{4.24}$$

$$\left.\begin{aligned} \tilde{V}_0^- &= -\frac{\mathrm{i}k_0^2p_0^-}{\omega_0\rho^-}\left[\eta - \frac{1}{\varkappa^-}\frac{1}{1+\rho^-(v^-)^{1/2}}\exp\left(\varkappa^-\eta\right)\right] + D^-, \\ D^- &= v_w - \frac{\mathrm{i}k_0^2a}{\omega_0\rho^-}\left(p_1^- - \frac{\omega_1}{\omega_0}p_0^-\right) \quad \text{with} \quad \varkappa^\pm = \left(-\mathrm{i}\omega_0/v^\pm\right)^{1/2}. \end{aligned}\right\} \tag{4.25}$$

The leading-order kinematic and pressure-jump conditions then provide two relations,

$$-\frac{\mathrm{i}k_0^2a}{\omega_0\rho^-}p_0^- = -\mathrm{i}\omega_0 f_0, \quad p_0^- = \gamma_0k_0^2f_0, \tag{4.26}$$

which show that the main-order frequency of the capillary waves is

$$\omega_0 = \pm k_0^2\left(a\gamma_0/\rho^-\right)^{1/2}, \tag{4.27}$$

where the sign determines the direction of the wave propagation. The disturbance decay rate,

$$\omega_{1i} = -\frac{(v^-)^{1/2}}{2^{3/2}} \frac{|k_0|\gamma_0^{1/4}}{a^{3/4}(\rho^-)^{1/4}} \left(1 + \frac{1}{1+\rho^-(v^-)^{1/2}}\right), \tag{4.28}$$

is fixed by the interfacial conditions at the next order.

The calculation leading to (4.28) shows that the capillary-wave decay is affected by the upper flow via the main-order interface displacement which contributes to the pressure variation in the main boundary layer and consequently alters the pressure within the film.

4.3. *Resonant amplification of TS waves*

The limit solutions for both the TS modes in §4.1 and the damped capillary waves in §4.2 must be reconsidered when the surface tension coefficient is close to the critical value $\gamma_c = \rho^-/a$. Suppose that $\gamma_0 = \gamma_c + \varepsilon^{1/2}\gamma_1$, where $\gamma_c = \rho^-/a$ and the detuning parameter γ_1 is of $O(1)$. As before, the small parameter ε is related to the value of the (large) wavenumber, $k = \varepsilon^{-1}k_0, k_0 = O(1)$. The frequency and the film-flow components expand in the form

$$\omega = \varepsilon^{-2}\omega_0 + \varepsilon^{-3/2}\omega_1 + \varepsilon^{-1}\omega_2 + \ldots, \quad \bar{u}^- = \varepsilon^{-1/2}u_0^- + u_1^- + \varepsilon^{1/2}u_2^- + \ldots, \tag{4.29}$$

$$[\bar{p}^-, \bar{v}^-] = \varepsilon^{-3/2}[p_0^-, v_0^-] + \varepsilon^{-1}[p_1^-, v_1^-] + \varepsilon^{-1/2}[p_2^-, v_2^-] + \ldots . \tag{4.30}$$

The velocities u_0^-, v_0^- and u_1^- can be related to the pressure terms using (4.8), whereas in the solution for v_1^- the Stokes-layer contribution must be dropped. The effect of the Stokes layer is felt at the next order, where we have

$$v_2^- = \frac{\mathrm{i}k_0^2}{\varkappa^-\omega_0\rho^-}p_0^- - \frac{\mathrm{i}k_0^2}{\omega_0\rho^-}(\bar{Y} + a)\left[-\frac{\omega_1}{\omega_0}p_1^- + \left(\frac{\omega_1^2}{\omega_0^2} - \frac{\omega_2}{\omega_0}\right)p_0^- + p_2^-\right]. \tag{4.31}$$

The upper-flow expansions acquire the form

$$\left.\begin{aligned} \bar{u}^+ &= A_0 + \varepsilon^{1/2}A_1 + \varepsilon A_2 + \ldots, \\ \bar{v}^+ &= \varepsilon^{-2}\left(-\mathrm{i}k_0A_0\tilde{Y}\right) + \varepsilon^{-3/2}\left(-\mathrm{i}k_0A_1\tilde{Y} + \mathrm{i}\omega_1A_0\right) \\ &\quad + \varepsilon^{-1}\left(-\mathrm{i}k_0A_2\tilde{Y} + \mathrm{i}\omega_1A_1 - \mathrm{i}(k_0u_{00} - \omega_2)A_0\right) + \ldots, \\ \bar{p}^+ &= \varepsilon^{-1}|k_0|A_0 + \varepsilon^{-1/2}|k_0|A_1 + |k_0|A_2 + \ldots, \end{aligned}\right\} \tag{4.32}$$

with $\tilde{Y} = \varepsilon\bar{Y} = O(1)$ and $\omega_0 = k_0|k_0|$. In the expansions for the interfacial boundary layers,

$$\bar{u}^\pm = \varepsilon^{-1/2}\tilde{U}_0^\pm(\eta) + \ldots, \quad \bar{v}^\pm = \varepsilon^{-3/2}v_0^-(0) + \varepsilon^{-1}v_1^-(0) + \varepsilon^{-1/2}\tilde{V}_0^\pm(\eta) + \ldots, \tag{4.33}$$

the crucial terms $\tilde{V}_0^\pm$ are given by the capillary-wave solution (4.24), (4.25) with D^- replaced by $v_2^-(0)$.

To illustrate the matching procedure for the current regime, consider the leading-order pressure-jump condition, namely

$$-\mathrm{i}\omega_0 p_0^- = k_0^2\gamma_c v_0^-(0). \tag{4.34}$$

With the value of $v_0^-(0)$ found from the leading coefficient in (4.8), this yields

$$\omega_0^2 = k_0^4\gamma_c a/\rho^-. \tag{4.35}$$

The last result will be compatible with the earlier derived formula $\omega_0 = k_0|k_0|$ only if

$\gamma_c = \rho^-/a$, as expected. A similar procedure applied at the next approximation leads then to the quadratic equation

$$2\gamma_c\omega_1^2 - \gamma_1 k_0^2\omega_1 + k_0^2|k_0| = 0, \tag{4.36}$$

for the first frequency correction ω_1 in terms of the detuning parameter γ_1. Assuming a real solution for ω_1, the disturbance growth/decay rate,

$$\omega_{2i} = \left(\frac{|k_0|}{\omega_1^2} - 2\frac{\gamma_c k_0^2}{\omega_0^2}\right)^{-1} \mathrm{Im}\left(\frac{1}{\varkappa^-}\right) \frac{k_0^2\gamma_c}{a\omega_0}\left(1 + \frac{1}{1+\rho^-(\nu^-)^{1/2}}\right), \tag{4.37}$$

is found from the higher-order balances. Here Im stands for the imaginary part.

The first frequency correction in (4.36) remains real only for sufficiently strong detuning. In the range $\gamma_1^2 < 8|k_0|\gamma_c$, i.e. when γ_0 is close to the critical value γ_c, the roots of the quadratic become complex, hence instability with the growth rate $\omega_{1i} = |k_0|(4\gamma_c)^{-1}\left(8|k_0|\gamma_c - \gamma_1^2\right)^{1/2}$ emerges. The instability results from the crossing of the real solutions of (4.36) when $|\gamma_1|$ is large and decreases, one of the solutions being the TS and the other the capillary-wave frequency correction. A more delicate analysis in the neighbourhood of the cut-off points $\gamma_{1c} = \pm\left(8|k_0|\gamma_c\right)^{1/2}$ is required in order to establish which of the two neutral (at this approximation) modes loses stability; however our computations in §3 point to the TS wave as being the less stable one. Indeed, when $\gamma_1 = 0$ the growth rate is found to be $\omega_{1i} = |2k_0|^{3/2}\gamma_c^{-1/2}$, hence in the unscaled form we have

$$\omega_i = \tfrac{1}{2}\left(2a/\rho^-\right)^{1/2}|k|^{3/2} + O(k) \quad \text{as} \quad |k| \to \infty. \tag{4.38}$$

Comparison of (4.38) with computations is shown in figure 4(*c*).

4.4. *The Hooper & Boyd mode*

Computations in §3 demonstrate the appearance of strong short-wave instability in the flow with a less viscous film fluid. Here we shall show that this mode is in fact related to a high-Reynolds-number long-wave instability of a piecewise profile examined earlier in Hooper & Boyd (1987). The mode is characterized by a small real part of the phase speed; in the regimes considered here and in §3 it generally remains below the interfacial velocity.

The frequency expansion is taken in the form

$$\omega = \varepsilon^{-1}\omega_0 + \varepsilon^{-1/2}\omega_1 + \ldots \quad \text{when} \quad k = \varepsilon^{-1}k_0, \quad k_0 = O(1). \tag{4.39}$$

On setting $\gamma_0 = Fr_0^{-1} = 0$, the disturbance in the film expands as

$$\bar{u}^- = \varepsilon^{-1}u_0^- + \varepsilon^{-1/2}u_1^- + \ldots, \quad \bar{v}^- = \varepsilon^{-2}v_0^- + \varepsilon^{-3/2}v_1^- + \ldots, \tag{4.40}$$

and then the common expansion,

$$\bar{p}^{\pm} = \varepsilon^{-1}p_0 + \varepsilon^{-1/2}p_1 + \ldots \tag{4.41}$$

holds for the pressure. The leading terms in (4.40) are given in (4.8) with p_0^- replaced by p_0. In the next approximation we have

$$u_1^- = \frac{k_0}{\omega_0\rho^-}\left(p_1 - \frac{\omega_1}{\omega_0}p_0\right) - \frac{\mathrm{i}}{\omega_0}\lambda^- v_w, \tag{4.42}$$

$$v_1^- = -\mathrm{i}k_0\left(\bar{Y} + a\right)\left[\frac{k_0}{\omega_0\rho^-}\left(p_1 - \frac{\omega_1}{\omega_0}p_0\right) - \frac{\mathrm{i}}{\omega_0}\lambda^- v_w\right] + v_w, \tag{4.43}$$

with v_w given by (4.10).

In the upper part of the flow with $\bar{Y} = O(1)$ the expansions are

$$\bar{u}^+ = A_0 + \ldots, \quad \bar{v}^+ = \varepsilon^{-2}(-\mathrm{i}k_0 p_0) + \varepsilon^{-3/2}(-\mathrm{i}k_0 p_1) + \ldots . \tag{4.44}$$

In the interfacial viscous layer the solution of §4.2 can be used, with the conclusion that the viscous layers do not alter the main-order vertical velocity. Hence the match between v_0^- and the leading term in $\bar{v}^+$ gives

$$\omega_0 = k_0 a/\rho^-. \tag{4.45}$$

To find the first complex-valued frequency correction matching at the next order is required. After some algebra we derive the formula

$$\omega_{1i} = \frac{1}{\sqrt{2}}(1 - v^-)\left(\frac{k_0}{a\rho^- v^-}\right)^{1/2} - \left(\frac{k_0}{a\rho^-}\right)^{1/2} \frac{(1-\rho^-)^2 (v^-)^2}{(1-v^-)^{3/2}\left(1 + \rho^- (v^-)^{1/2}\right)}. \tag{4.46}$$

The result of (4.46) is equivalent to the long-wave limit of (3.32*c*) in Hooper & Boyd (1987).

A comparison with the full numerical solution is shown in figure 2(*f*). According to (4.39), the estimate for the growth rate is $\omega_i \sim k^{1/2}$ as $k \to \infty$; however a better agreement is found if we allow a constant vertical shift of the solution curve, thus implying a next-order correction of $O(1)$ in the limit solution.

5. Instabilities of very viscous films

The interfacial viscosity difference in the case of a more viscous film gives rise to the long-wave instability illustrated in figures 2(*h–j*). The focus in this section is on limiting properties of this mode, first with respect to small wavenumbers in the flow with $O(1)$ parameters, extended eventually to highly viscous films for the disturbance wavenumbers covering the entire unstable spectrum. The limit properties of the TS modes are considered in §5.4.

5.1. *The long-wave interfacial instability*

Here we derive a long-wave asymptotic solution for the computational curves in figures 2(*h–j*). Suppose that $k = \varepsilon k_0$, with $\varepsilon \to 0$ and $k_0 = O(1)$. Since in the limit the disturbance frequency is small, we expect the perturbed motion in the upper fluid to be viscous and quasi-stationary. This leads to the expansions,

$$\bar{u}^+ = A_0 + \varepsilon^{4/3}\tilde{u}^+\left(\tilde{Y}\right) + \ldots, \quad \bar{v}^+ = \varepsilon^{2/3}\left(-\mathrm{i}k_0 A_0 \tilde{Y}\right) + \varepsilon^2 \tilde{v}^+\left(\tilde{Y}\right) + \ldots, \tag{5.1}$$

$$\bar{p}^+ = \varepsilon |k_0| A_0 + \ldots, \tag{5.2}$$

$$\omega = \varepsilon k_0 u_{00} + \varepsilon^{8/3}\omega_1 + \ldots \quad \text{as} \quad \varepsilon \to 0, \tag{5.3}$$

with $\tilde{Y} = \varepsilon^{1/3}\bar{Y}$ of $O(1)$ and the growth rate assumed to be of order $\varepsilon^{8/3}$, as will be verified *a posteriori*. The controlling disturbance equations,

$$\mathrm{i}k_0 \tilde{Y}\tilde{u}^+ + \tilde{v}^+ = -\mathrm{i}k_0 |k_0| A_0 + \tilde{u}^{+\prime\prime}, \quad \mathrm{i}k_0 \tilde{u}^+ + \tilde{v}^{+\prime} = 0, \tag{5.4}$$

can be solved, subject to $\tilde{v}^+(0) = 0$, in terms of the Airy function Ai. The result required here is that

$$\tilde{u}^{+\prime}(0) = (\mathrm{i}k_0)^{2/3} |k_0| A_0 \mathrm{Ai}(0) \left[\mathrm{Ai}'(0)\right]^{-1}. \tag{5.5}$$

In the film the effect of the pressure gradient is small, hence

$$\bar{u}^- = \varepsilon^{5/3} A^- \left(\bar{Y} + a\right) + \ldots, \quad \bar{v}^- = \varepsilon^{8/3} \left[-\tfrac{1}{2} A^- \mathrm{i} k_0 \left(\bar{Y} + a\right)^2\right] + \ldots . \tag{5.6}$$

The use of the interfacial conditions allows the constant A^- to be expressed in terms of the shear perturbation (5.5) and yields eventually the formula for the frequency correction,

$$\omega_1 = \frac{1 - \lambda^-}{\rho^- v^-} \frac{a^2}{2} \frac{\mathrm{Ai}\,(0)}{|\mathrm{Ai}'\,(0)|} \left(\mathrm{i} k_0\right)^{2/3} k_0 |k_0|. \tag{5.7}$$

The imaginary part of ω_1 is positive when $1 - \lambda^- = 1 - (\rho^- v^-)^{-1} > 0$, that is instability results if the dynamic viscosity of the lower fluid is greater than in the main boundary layer.

Comparison of the asymptotic formula with the full numerical solution is made in figure 2(*j*). For the flow with $a = 1, \rho^- = 1, v^- = 5$, we have $\lambda^- = 0.2, u_{00} = a\lambda^- = 0.2$, hence

$$c_r = \omega_r / k = 0.2 + \ldots, \quad \omega_i = 0.09503 k^{8/3} + \ldots \quad \text{as} \quad k \to 0+. \tag{5.8}$$

Here the first relation shows that the long-wave disturbance is in fact a slowly growing wave propagating with the basic-state interfacial speed. The growth rate in (5.7) or (5.8) should be compared with the long-wave formulae $\omega_i = O\left(k^2\right)$ and $\omega_i = O\left(k^{4/3}\right)$ obtained in a similar regime but for different flows by Yih (1967) and Hooper (1985), respectively. The higher power of k in our case is due to the inviscid potential flow in the upper zone of the interaction region, as reflected in the coefficient $|k_0|$ in (5.7). The effect of viscous/inviscid interaction in the present long-wave limit is rather weak, for the pressure in the boundary-layer formulation (5.4) acts as a given function (even though the main-order term A_0 is essentially arbitrary). Nevertheless the specific form of the interaction proves to be significant for long waves. Note also that surface tension has no effect on the small-k disturbance unless γ_0 is made sufficiently large to affect the shear-stress-dominated flow in the film.

5.2. *Interfacial instability for increased film viscosity*

The growth rate curves in figure 2(*h*) show a distinct maximum of the interfacial instability shifted towards larger wavenumbers when λ^- becomes small. Keeping in mind applications in which the viscosity ratio is large, we shall now examine the entire spectrum of the interfacial instability (including the range of maximum growth rates) on the assumption that $v^- \to \infty$. For simplicity the density of the lower fluid is taken of $O\,(1)$, although the final relations are found to be valid in a wider density range, in accord with the observation in the previous subsection and in earlier studies that the interfacial mode should be dependent on the dynamic rather than kinematic viscosity properties (a more complete account of the limit solutions with large ρ^- and v^- will be given in a forthcoming paper, see also Tsao *et al.* 1997).

Consider first the case $v^- \gg 1$ for a finite wavenumber k and parameters a, γ_0, Fr_0 fixed at $O\,(1)$. As in §5.1, the boundary-layer part of the disturbance is then governed by viscous quasi-steady equations, this time in the layer $\bar{Y} = O\,(1)$, with the leading-order terms of the form

$$[\bar{u}^+, \bar{v}^+, \bar{p}^+, \bar{A}] = [u_0^+, v_0^+, |k| A_0, A_0] + O\left(1/v^-\right), \quad \omega = \omega_1 / v^- + \ldots . \tag{5.9}$$

The controlling equations for u_0^+, v_0^+ are as in (5.4) with k_0 replaced by k, the crucial

difference being that now the viscous/inviscid interaction is present at the main order, as is reflected in the outer-edge condition, $u_0^+(\infty) = A_0$. The requirement of zero vertical velocity on approach to the interface is appropriate here; however the subsequent match with the film flow shows that in the current regime neither the streamwise velocity nor the tangential stress at $\bar{Y} = 0$ can be chosen in advance. Therefore we take $v_0^+(0) = 0$, $u_0^+(0) = Q$, $u_0^{+\prime}(0) = L$, with the constants Q, L unknown at the moment. Solving (5.4) with the stated boundary conditions we find two relations for p_0^+, Q and L, namely

$$L = -\frac{3\mathrm{Ai}(0)(\mathrm{i}k)^{2/3}|k|}{3|\mathrm{Ai}'(0)| + (\mathrm{i}k)^{1/3}|k|}Q, \quad p_0^+ = \frac{3|\mathrm{Ai}'(0)||k|}{3|\mathrm{Ai}'(0)| + (\mathrm{i}k)^{1/3}|k|}Q. \tag{5.10}$$

The film flow at leading order is now driven by a combination of the interfacial shear stress and pressure, hence

$$\left[\bar{u}^-, \bar{v}^-, \bar{p}^-, \bar{f}\right] = \left[u_0^-/v^-, v_0^-/v^-, p_0^-, f_0\right] + \ldots, \tag{5.11}$$

$$u_0^- = \frac{1}{2}\frac{\mathrm{i}kp_0^-}{\rho^-}\left(\bar{Y} + a\right)^2 + A^-\left(\bar{Y} + a\right), \tag{5.12}$$

$$v_0^- = \frac{1}{6}\frac{k^2p_0^-}{\rho^-}\left(\bar{Y} + a\right)^3 - \tfrac{1}{2}\mathrm{i}kA^-\left(\bar{Y} + a\right)^2, \tag{5.13}$$

where the constant A^- can be determined using the interfacial conditions. The latter also supply the formula

$$\omega_1 = \frac{ka}{\rho^-} - \frac{\mathrm{i}k^2a^3}{3\rho^-}\left(\gamma_0k^2 + \frac{\rho^- - 1}{Fr_0}\right) + \frac{a^2}{2\rho^-}\frac{3\mathrm{Ai}(0)\,k|k|\,(\mathrm{i}k)^{2/3} + 2\mathrm{i}ak^2|k||\mathrm{Ai}'(0)|}{3|\mathrm{Ai}'(0)| + (\mathrm{i}k)^{1/3}|k|} \tag{5.14}$$

for the disturbance frequency.

The first term in (5.14) corresponds to a neutral wave with the phase speed of the main flow at the interface. The second term reflects the stabilizing influence of gravity and the surface tension. The feature not examined in computations in §3 (where the flow with a more viscous fluid in the film was assumed to have $Fr_0 = \infty$) is the long-wave stabilization due to a stable density stratification. The instability in (5.14) is contained in the third term. If, for example, $k \to 0$ then the result of §5.1 is recovered provided that gravity can be neglected. If, on the other hand, $Fr_0^{-1} = \gamma_0 = 0$ and the wavenumber is large then instability persists for all k, including the limit as $k \to \infty$ where the asymptotic behaviour,

$$\omega_{1i} = a^3\left(2\rho^-\right)^{-1}|\mathrm{Ai}'(0)|k^{5/3} + \ldots, \quad k \gg 1 \tag{5.15}$$

holds for the growth rate.

According to (5.9) and (5.14), the disturbance growth rate decreases as v^- increases for a fixed wavenumber k. This trend can be seen in figure 2(h) for the values of k less than 3 or 4, approximately, when v^- is greater than 4 or 5. In order to be able to detect the growth-rate reduction on shorter waves a considerably larger film viscosity is needed (see also a realistic-flow example in the last section of the paper).

5.3. *Short interfacial waves*

Clearly the increased growth-rate maximum and the ultimate decay of extremely short waves illustrated in figure 2(h) is not covered by the analysis in the previous subsection. The appropriate scalings for an alternative limit description required when both v^- and k are large can be derived from a simple physical argument as follows.

When $k \gg 1$ and the upper-fluid velocity $\bar{u}^+$ (but not $\bar{A}$ as in the previous sections) is taken of $O(1)$, the requirement of the inertia/pressure/viscous shear balancing in the momentum equation for the disturbance just above the interface indicates that $\bar{Y} \sim k^{-1/3}$, $\bar{p}^+ \sim k^{-1/3}$. Provided that the interfacial pressure jump is not excessively large, the last estimate also holds for the pressure in the film, $\bar{p}^- \sim \bar{p}^+$; therefore velocities of a viscous pressure-driven disturbance in the film are estimated as $\bar{u}^- \sim k^{2/3}/(\rho^- v^-), \bar{v}^- \sim k^{5/3}/(\rho^- v^-)$, the former from the momentum equation, and the latter from mass conservation. The tangential velocity continuity suggests then that $\bar{f}$ and $\bar{u}^+$ must be of the same order of magnitude, i.e. $\bar{f} = O(1)$, so that the interfacial kinematic condition approximated for the lower fluid as $\bar{v}^- \sim \mathrm{i}\omega\bar{f}$ gives $\omega \sim k^{5/3}/(\rho^- v^-)$. The argument so far follows the instability mechanism examined in §5.2, and in fact the estimate for the wave frequency above is of the form (5.15). Among several factors which can alter this scheme when the wavelength becomes sufficiently small, the first one to enter the reckoning proves to be due to temporal variations in the boundary-layer flow on the upper side of the interface (in addition to the unsteadiness already present in the interfacial kinematic condition). From the balance $-\mathrm{i}\omega\bar{u}^+ \sim \partial^2\bar{u}^+/\partial\bar{Y}^2$, valid in the viscous layer of thickness $\bar{Y} = O\left(k^{-1/3}\right)$ it then follows that $\omega = O\left(k^{2/3}\right)$. The last estimate, compared with the previously derived $\omega \sim k^{5/3}/(\rho^- v^-)$, shows that the wavenumber range for the new regime is $k = O(\rho^- v^-)$.

In accord with the estimates above we apply the scaling transformations, $k = v^- k_0, \bar{Y} = (v^-)^{-1/3}\tilde{Y}$, with $(\tilde{Y}, k_0)$ of $O(1)$, for the wavenumber and vertical coordinate, and seek the solution for the upper boundary layer in the form

$$\left[\bar{u}^+, \bar{v}^+, \bar{p}^+\right] = \left[u_0^+\left(\tilde{Y}\right), \left(v^-\right)^{2/3} v_0^+\left(\tilde{Y}\right), \left(v^-\right)^{-1/3} p_0^+\right] + \ldots, \quad \omega = \left(v^-\right)^{2/3}\omega_1 + \ldots . \tag{5.16}$$

The governing equations for the leading terms in (5.16) are

$$\left(-\mathrm{i}\omega_1 + \mathrm{i}k_0\tilde{Y}\right) u_0^+ + v_0^+ = -\mathrm{i}k_0 p_0^+ + u_0^{+\prime\prime}, \quad \mathrm{i}k_0 u_0^+ + v_0^{+\prime} = 0. \tag{5.17}$$

Owing to the decreased wavelength the viscous/inviscid interaction condition for the upper flow reduces to the zero-displacement requirement, $u_0^+ \to 0$ as $\tilde{Y} \to \infty$. As in §5.2, the tangential slip velocity at the interface continues to play a significant part, and in addition the interface displacement turns out to be sufficiently strong to affect the vertical velocity in the upper fluid. The remaining boundary conditions on (5.17) are hence written as $u_0^+(0) = Q, v_0^+(0) = \Phi$, where the values of Q, Φ are determined below. In the film-flow expansions,

$$\left[\bar{u}^-, \bar{v}^-, \bar{p}^-\right] = \left[\left(v^-\right)^{-1/3} u_0^-\left(\bar{Y}\right), \left(v^-\right)^{2/3} v_0^-\left(\bar{Y}\right), \left(v^-\right)^{-1/3} p_0^-\right] + \ldots, \tag{5.18}$$

we find that

$$u_0^- = \frac{\mathrm{i}k_0 p_0^-}{\rho^-}\left[\tfrac{1}{2}\left(\bar{Y}+a\right)^2 - a\left(\bar{Y}+a\right)\right], \tag{5.19}$$

$$v_0^- = -\frac{(\mathrm{i}k_0)^2 p_0^-}{\rho^-}\left[\tfrac{1}{6}\left(\bar{Y}+a\right)^3 - \tfrac{1}{2}a\left(\bar{Y}+a\right)^2\right]. \tag{5.20}$$

The tangential stress at the interface in (5.19) must vanish in order to provide matching with the leading term in $\bar{u}^+$.

The kinematic condition satisfied for both upper and lower fluids in conjunction with the pressure-jump value yields two relations:

$$\Phi = -\frac{a^3 k_0^2}{3\rho^-}\left[p_0^+ - \left(\gamma_1 k_0^2 + \frac{\rho^- - 1}{Fr_1}\right) Q\right], \quad \Phi = \mathrm{i}\omega_1 Q. \tag{5.21}$$

On account of arbitrary normalization (for example, $Q = 1$) these can be regarded as giving a relation between the upper-flow pressure p_0^+ and the wave frequency ω_1. Then the interfacial velocities $u_0^+(0)$ and $v_0^+(0)$ can also be expressed in terms of ω_1. Note that the additional scaling

$$\gamma_0 = \left(v^-\right)^{-7/3}\gamma_1, \quad Fr_0 = \left(v^-\right)^{1/3} Fr_1 \tag{5.22}$$

was used for the surface tension and gravity to have the same order-of-magnitude effect as the interfacial pressure.

The required solution for the boundary-layer equations (5.17) can be found analytically in terms of the Airy function; however for our purposes a minor adjustment of the program used in §3 proved easier. Provided that surface tension and gravity are negligible the effects of density and film thickness variations are eliminated from the system by the change of variables

$$\left[k_0, \tilde{Y}, \omega_1, v_0^+, p_0^+, \Phi\right] \to \left[\beta k_0, \beta^{-1/3}\tilde{Y}, \beta^{2/3}\omega_1, \beta^{2/3} v_0^+, \beta^{-1/3} p_0^+, \beta^{2/3}\Phi\right], \tag{5.23}$$

where $\beta = \rho^-/a^3$. The frequency is then written in the form

$$\omega_1 = \frac{(\rho^-)^{2/3}}{a^2}\Omega_1\left(\frac{k_0 a^3}{\rho^-}\right) \quad \text{if} \quad \gamma_1 = Fr_1^{-1} = 0, \tag{5.24}$$

with Ω_1 independent of ρ^- or a. If, however, γ_1 and especially Fr_1 are retained then the dependence on the film density becomes far more complicated.

A few examples of the growth-rate curves obtained numerically for the current regime are shown in figure 6(a). The solution with $\rho^- = a = 1, \gamma_1 = Fr_1^{-1} = 0$ represents the function Ω_1. When the film density increases, the maximum growth rate appears at higher wavenumbers, in accord with (5.24). Gravity and surface tension tend to suppress interfacial modes. Further comparison in figure 6(b) is made in similarity variables. The rate of approach of the full numerical solutions of §3 to the high-viscosity limit is slow (in order to make the limiting trends more or less visible, computations for the full formulation had to be extended to much higher values of v^- than those presented in figure 2h).

We conclude that the flow regime considered in this section contains the most unstable part and the upper-branch neutral point in the interfacial wave spectrum.

5.4. *The TS instability*

The interfacial mode in §5.3 has increased maximum growth rates when the film viscosity is large (see also figure 2h). The aim of this subsection is to compare this effect with the TS-wave destabilization observed in similar circumstances in computations of §3 (see figure 2a). In order to make a direct comparison with the interfacial mode, the effects of surface tension and gravity are neglected here. Also the film density is taken to be of $O(1)$.

The key assumption in the following analysis is that the fastest growing TS instability occurs at increased wavenumbers when $v^- \gg 1$. Then starting from the disturbance structure described in §4.1 (for the case $v^- = O(1)$ and $k \gg 1$) we notice that the near-wall layer and also the viscous layer on the film side of the interface

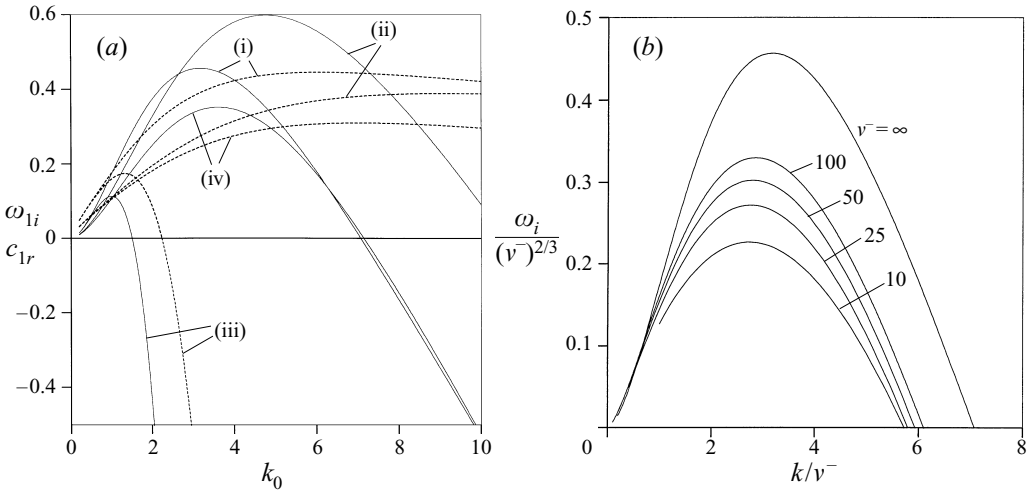

FIGURE 6. (*a*) Solutions of (5.17)–(5.21) with $a = 1$. (i) $\gamma_0 = Fr_0^{-1} = 0, \rho^- = 1$; (ii) $\gamma_0 = Fr_0^{-1} = 0, \rho^- = 1.5$; (iii) $\gamma_0 = 0.2, Fr_0^{-1} = 0, \rho^- = 1$; (iv) $\gamma_0 = 0, Fr_0^{-1} = 0.2, \rho^- = 1.5$; (*b*) Comparison between the limiting solution (5.24), $\nu = \infty$, and the growth rates computed in the full formulation for the film parameters $\rho^- = 1, \gamma_0 = Fr_0^{-1} = 0, a = 1$.

both have the thickness scale $O\left(\left(\nu^-/\omega\right)^{1/2}\right)$, where $\omega \sim k^2$. Hence for a sufficiently large film viscosity a new structure emerges as the two viscous layers fill the entire film, that is when $\nu^- \sim k^2$. We shall verify afterwards that this new regime covers the strongest TS instability.

In keeping with the estimates above we take

$$k = \varepsilon^{-1}k_0, \quad \nu^- = \varepsilon^{-2}\nu_0^-, \quad \omega = \varepsilon^{-2}\omega_0 + \varepsilon^{-1}\omega_1 + \ldots, \tag{5.25}$$

with k_0 and ν_0^- of $O(1)$. The boundary-layer part of the disturbance is written in the form

$$\bar{u}^+ = A_0 + \varepsilon A_1 + \ldots, \quad \bar{v}^+ = \varepsilon^{-2}\left(-\mathrm{i}k_0 A_0 \tilde{Y}\right) + \varepsilon^{-1}\left(-\mathrm{i}k_0 A_1 \tilde{Y} + \mathrm{i}\omega_1 A_0\right) + \ldots, \tag{5.26}$$

$$\bar{p}^+ = \varepsilon^{-1}|k_0|A_0 + |k_0|A_1 + \ldots, \tag{5.27}$$

in the region $\tilde{Y} = \varepsilon\bar{Y} = O(1)$, together with the familiar result for the leading-order frequency, $\omega_0 = k_0|k_0|$. The main disturbance terms in the film-flow expansions,

$$\bar{u}^- = u_0^- + \ldots, \quad \bar{v}^- = \varepsilon^{-1}v_0^- + \ldots, \quad \bar{p}^- = \varepsilon^{-1}p_0^- + \ldots, \tag{5.28}$$

satisfy the equations,

$$-\mathrm{i}\omega_0 u_0^- = -\frac{\mathrm{i}k_0}{\rho^-}p_0^- + \nu_0^- u_0^{-\prime\prime}, \quad \mathrm{i}k_0 u_0^- + v_0^{-\prime} = 0. \tag{5.29}$$

The appropriate boundary conditions are the wall constraints and the requirement of zero interfacial shear (the latter due to the increased film viscosity), hence $u_0^-(-a) = v_0^-(-a) = u_0^{-\prime}(0) = 0$. The interfacial matching of (5.26), (5.27) with the solution for the film yields the first frequency correction,

$$\omega_1 = -\frac{k_0 a}{\rho^-}\left[1 - \frac{1}{\varkappa_0^- a}\tanh\left(\varkappa_0^- a\right)\right], \quad \varkappa_0^- = \left(-\frac{\mathrm{i}k_0^2}{\nu_0^-}\right)^{1/2}. \tag{5.30}$$

The imaginary part of ω_1 corresponding to the TS-wave growth rate is illustrated in

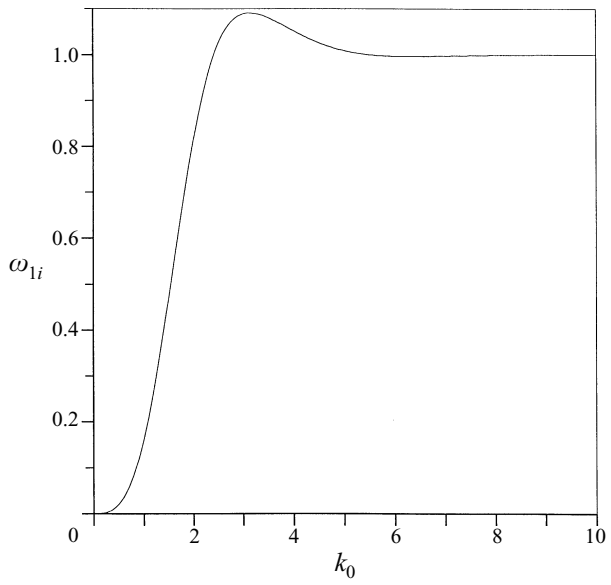

FIGURE 7. The scaled growth rate ω_{1i} versus k_0 from the solution (5.30) with $a = 1, \rho^- = 1, v_0^- = 1$.

figure 7. The diagram shows a maximum in the middle of the chosen wavenumber range.

In the unscaled variables (ω, v^-, k) the largest growth rate is estimated as $\omega_i = O\left((v^-)^{1/2}/\rho^-\right)$, when $k = O\left((v^-)^{1/2}\right), v^-$ is large, and ρ^- can be arbitrary but not extremely large or small to affect the disturbance structure. If, for a given large v^-, the wavenumber k is taken beyond the range of validity of (5.30) then the growth rate is evaluated by the limit relations

$$\omega_i = \frac{1}{\rho^-}\left(\frac{v^-}{2}\right)^{1/2} + \ldots \quad \text{when} \quad k \gg \left(v^-\right)^{1/2}, \tag{5.31}$$

$$\omega_i = \frac{a^3}{3\rho^- v^-}k^2|k| + \ldots \quad \text{when} \quad k \ll \left(v^-\right)^{1/2}. \tag{5.32}$$

In a similar large-viscosity regime the largest growth rate of interfacial modes was found to be of $O(\rho^- v^-)^{2/3}$ at k of $O(\rho^- v^-)$. Thus the interfacial waves are more unstable; however the difference is not particularly large for moderately high values of the film viscosity.

6. Discussion

As already mentioned in the Introduction, several high-Reynolds-number approximations have been developed previously with the aim of understanding instability mechanisms operational in two-fluid flows. The asymptotic analysis in this paper has two main novel features. First, regardless of the asymptotic nature of our solutions, the disturbance components in the two fluids remain fully coupled at the interface in the sense that no further simplifications in addition to those made in the governing equations are introduced in the interfacial conditions. As a consequence, the starting boundary-value problem (2.15), (2.18)–(2.25) retains both the kinematic (via the interfacial conditions) and the dynamic (via the momentum equations) nonlinearities

inherent in the full Navier–Stokes formulation. At the same time the viscous/inviscid interaction formulation proves to be sufficiently simple to allow a wide parameter analysis at a relatively low computational expense, as we show in §3. In this respect the model may prove useful in future nonlinear studies. An additional decoupling between the disturbance components introduced when certain parameters of the fluids become large or small should also be interesting to examine at a nonlinear level (see also Tsao *et al.*, 1997). Secondly, to capture both the TS and the interfacial instability mechanisms within one model the interface in this study is assumed to lie within the near-wall viscous layer. In this aspect the analysis here differs from other multi-deck studies (see the Introduction).

The effect of the film thickness variation was almost entirely beyond the scope of this work, although in many places it can be assessed easily from the limit solutions, see e.g. (4.16), (5.24), (5.30). The overall impression is that the thickness effects should be linked with the study of upper-branch instabilities and/or with the disturbance structures arising in the continuation of the lengthscale shortening described in §§5.3, 5.4. For shorter TS waves and thinner films, for example, a generalization of the solution in §4 is required when the film is buried in the Stokes layer; however the same generalized solution will hold for the entire neighbourhood of the upper neutral branch. Increased film thickness leads eventually to the short-wave critical layer being located near or below the interface. At this stage the curvature of the mean profile may become significant. All this is left for future study.

Numerical solutions presented in §3 indicate that in many cases the growth-rate maxima for both the TS and interfacial instabilities are finite and they are achieved at finite wavenumbers (e.g. in figures 2*a*,*h*, 3*a*,*c*). For such flows the temporal development of disturbances initiated by point or distributed sources can be studied using time-marching computations for the viscous/inviscid interaction equations. In certain regimes, however, (see in figure 2*a*, the flow with $\lambda^- > 1$, and also the resonant case in figure 4*a*) the strongest instability is found to occur beyond the wavenumber range covered by the present theory and therefore the initial-value analysis may prove inadequate.

Among the main goals of this work was a comparison between the growth rates of the TS and interfacial modes. We are not aware of any qualitative experimental data on the transitional-flow regimes in the boundary-layer/liquid film configuration which could be used for testing the present theory (but see below). One of the main conclusions of this work however, namely the significance of a strong competition between the two modes, seems to be in line with the known results for certain channel flows (see the experimental data in Charles & Lilleleht 1965; Kao & Park 1972, and the theory in Yantsios & Higgins 1988).

An important and rather peculiar effect found in this work is the flow destabilization due to the closeness of growing TS and damped interfacial disturbances. A linear resonance between the two modes was described as a possibility in Miles (1962); however his predictions referred to destabilization of interfacial modes. We do not observe such an effect probably because of the small film thickness assumed here. In the current two-dimensional theory the resonant amplification is found to be most efficient for a specific choice of the surface tension coefficient. A three-dimensional (oblique-wave) extension of the theory should prove interesting, for then a similar resonance is likely to occur under more natural conditions, i.e. with fixed film-flow properties but variable wave angle. Another possibility, namely a TS/gravity mode crossing was conjectured by Akylas (1982). Although his finite-Reynolds-number calculation strictly requires an exact intersection of neutral curves, the actual theory

was constructed more in the vein of an asymptotic treatment where, not dissimilar from the results of the present paper, the resonance conditions would have to be met only at leading order in powers of a small parameter (the inverse wavenumber in our case). Note also that as far as infinitesimal disturbances are concerned the distinction between capillary and gravity waves may not be evident until the scaled surface tension and Froude number are replaced by realistic numerical coefficients. In particular, the resonance theory of §4.3 applies also to gravity waves provided that $\gamma_0 = 0, Fr_0^{-1} \to \infty$, and the small parameter ε is expressed in terms of the Froude number.

Most of the experiments reported in literature deal with a turbulent main flow and laminar or turbulent flow in the film; see, e.g., Hanratty & Hershman (1961), Cohen & Hanratty (1965), Craik (1966), Andreussi, Asali & Hanratty (1985), Bruno & McCready (1988). However, in qualitative agreement with the results in this paper, mixed laminar–turbulent regimes were observed simultaneously with interfacial instabilities by Hanratty & Engen (1957), Charles & Lilleleht (1965), and Kao & Park (1972) in channels and by Ludwieg & Hornung (1989) in boundary layers. For a thin-film configuration, it appears that laminar–turbulent transition in the main body of fluid may occur before or after initiation of interfacial instabilities; however only if the film viscosity and density differ considerably from the main-fluid parameters can the growth of turbulence be distinguished from the activity of interfacial modes. Indeed, for order-one parameters of the two fluids our computations in §3 predict comparable growth rates of the TS and interfacial waves.

The set of experiments most closely related to the flow regimes in this paper is described in Ludwieg & Hornung (1989, hereafter referred to as LH). They studied initial stages in the formation of a skin-friction-line pattern during an oil-film visualization experiment. In the experiment a flat plate is covered with a uniform oil film; the film thickness before the test is $h_* = 0.015\,\mathrm{cm}$, the oil viscosity $\mu_{*\mathrm{oil}} = 2.9\,\mathrm{g\,cm^{-1}\,s^{-1}}$, the surface tension coefficient $\gamma_* = 0.02\,\mathrm{N\,m^{-1}}$ (as in §2 an asterisk is used to mark dimensional quantities). After the air flow is set up tangentially to the plate, two- and three-dimensional ripples begin to appear on the oil surface indicating the development of interfacial instabilities. Experimental results which will be used for comparison with the present theory are summarised in figure 4 of LH, the case of a pure laminar boundary layer with the air speed $36\,\mathrm{m\,s^{-1}}$.

The flow parameters in the experiment suggest that the waviness at the interface is due to the long-wave interfacial mode described in §5.2. The Reynolds number in the air flow is $Re_{LH} = U_*\delta_*/\nu_{*\mathrm{air}} = 2000$, where δ_* is the dimensional boundary-layer thickness. Since, according to LH, the Mach number in the flow is $\lesssim 0.25$, it seems reasonable to take the standard data at 20°C for the air density $\rho_{*\mathrm{air}} = 1.205 \times 10^{-3}\,\mathrm{g\,cm^{-3}}$ and kinematic viscosity $\nu_{*\mathrm{air}} = 0.15\,\mathrm{cm^2\,s^{-1}}$ (these parameters are not given in LH). The boundary-layer thickness is then evaluated as $\delta_* = 0.083\,\mathrm{cm}$. For the unperturbed boundary layer LH use a Pohlhausen polynomial approximation with the scaled wall shear equal to 2. Hence the dimensional boundary-layer thickness may be written in the form

$$\delta_* = \frac{2}{0.332} L_* Re^{-1/2}, \tag{6.1}$$

where L_* is the distance from the leading edge to the observation station and $Re = U_* L_*/\nu_{*\mathrm{air}}$ is the Reynolds number used in this paper. The number coefficient in (6.1) is introduced in order to rescale the wall shear given by LH to the Blasius-flow

value $\lambda^+ = 0.332$. With the estimate for the boundary-layer thickness given above the relation (6.1) provides the values,

$$L_* = 4.59\,\text{cm}, \quad Re = 110227 \tag{6.2}$$

for the distance from the leading edge and the Reynolds number respectively.

For the comparison the disturbance wavelength experimentally measured in LH and the corresponding result of our theory are converted into dimensional form. A cloud of experimental dots in figure 4 of LH can be characterized by

$$\alpha_+ \approx 0.035, \quad 12.65 \lesssim h_+ \lesssim 31.65, \quad 1800 \lesssim \sigma_+ \lesssim 3500. \tag{6.3}$$

Here α_+, h_+, σ_+ are non-dimensional parameters defined by the system of relations (18) in LH. From the first two equations of that system we find that the dimensional disturbance wavenumber α_* and the film thickness h_* are related by $\alpha_* h_* = \alpha_+ h_+$. Hence, using (6.2) and the estimate $h_* = 0.015\,\text{cm}$ for the film thickness, the disturbance wavenumber can be put in the range $29.52 \lesssim \alpha_* \lesssim 73.85\,\text{cm}^{-1}$, that is the dimensional wavelength $\lambda_* = 2\pi/\alpha_*$ is evaluated as

$$0.085 \lesssim \lambda_* \lesssim 0.213\,\text{cm}. \tag{6.4}$$

A somewhat different estimate follows from the first and third relations in (18) of LH which can be combined into $\alpha_+/\sigma_+ = \alpha_* \nu_{*\text{air}}^2 \rho_{*\text{air}} / (2\gamma_*)$. Using the parameter ranges (6.3) and the standard air density and viscosity we obtain that

$$14.75 \lesssim \alpha_* \lesssim 28.687\,\text{cm}^{-1}, \quad 0.219 \lesssim \lambda_* \lesssim 0.425\,\text{cm}. \tag{6.5}$$

We were unable to find the source of such a big difference between the two estimates (6.4) and (6.5), nor could we decide which of the two provides a better representation of the experimental measurements. The discrepancy may be due to our choice of the air parameters, to the interpretation of the film thickness as that before the test, or to some other factors. This introduces some uncertainty in the following calculation; nevertheless we shall proceed on the assumption that the estimates above reproduce the true orders of magnitude of the measured quantities.

Following the normalization introduced in §2 we find that in our notation $\gamma = 0.000279, \varepsilon_0 = Re^{-1/8} = 0.2343$, and then $\gamma_0 = \gamma \varepsilon_0^{-3} \left(\lambda^+\right)^{5/4} = 0.00547$, where the Blasius-flow wall shear $\lambda^+ = 0.332$ is included on account of the affine transformation (2.26). The scaled film thickness is then evaluated as $a = h_* L_*^{-1} \varepsilon_0^{-5} \left(\lambda^+\right)^{3/4} = 2.0256$. The disturbance growth rates were computed from the limit relation (5.14) and, for an independent verification, from the full formulation (3.3)–(3.8). The results are shown in figure 8, the solid and dashed curves, respectively. Note that the dashes are drawn for three almost indistinguishable solutions corresponding to the oil density $\rho_{*\text{oil}} = 0.1, 1$ and $10\,\text{g}\,\text{cm}^{-3}$. In all three cases the limit formula (5.14) gives a good approximation to the full solution. The maximum at $k_{max} \approx 5.945$ in figure 8 provides the wavenumber of the most amplified disturbance. The corresponding dimensional wavelength $\lambda_* = L_* \varepsilon_0^3 \left(\lambda^+\right)^{-5/4} 2\pi/k_{max}$ is then found to be $\lambda_* \approx 0.245\,\text{cm}$. This theoretical value is just above the range (6.4) and falls within the bounds of (6.5). Keeping in mind the approximate nature of our theory the agreement seems to be encouraging.

On the qualitative side another observation deserves a brief mention here. In the experiment the laminar–turbulent transition in the air boundary layer starts as an abrupt three-dimensional process by-passing the usual long and slow route of initially two-dimensional TS-wave amplification. This points to the significance of shorter-

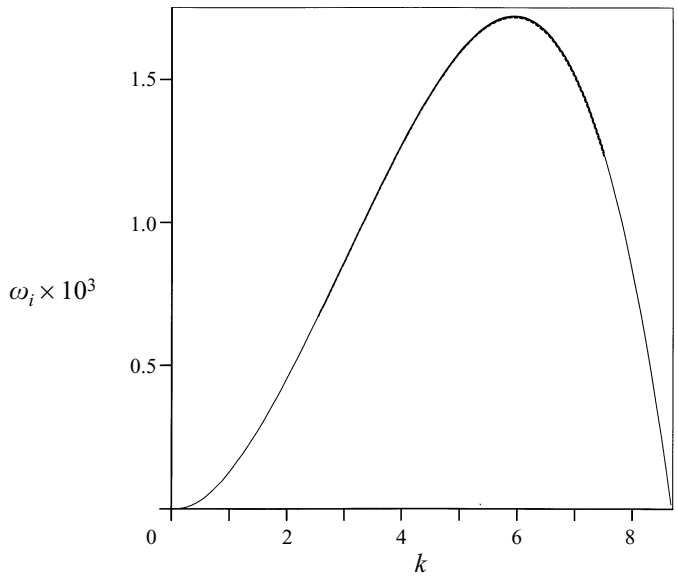

FIGURE 8. The growth rate ω_i versus k for the experimental conditions in LH. Solid line: the limit formula (5.14); three dashed curves were plotted in the figure for the full triple-deck solutions with various densities of the oil film.

scale dynamics in the transitional boundary layer, in agreement with the theoretical conclusion that the most amplified TS waves on very viscous films have a considerably reduced wavelength; see §5.4. Further theory and experiment are required in order to be more specific on this score.

The author is grateful to the participants of the Applied Mathematics Seminar of Hull University for a fruitful discussion, especially on the applicability of the present and related models to condensation problems, to Professors S. N. Brown and F. T. Smith and Drs R. I. Bowles and S. J. Clarke for their attention to this work and frequent advice, and to the referees for many helpful comments and suggestions.

Appendix. Numerical method

Eliminating $\bar{u}^{\pm}$ from the momentum equations and making the substitutions

$$\bar{v}^{+} = -\mathrm{i}k\bar{Y} + N^{+} + \hat{v}^{+}\left(\bar{Y}\right), \quad \bar{v}^{-} = L^{-}z + N^{-} + \hat{v}^{-}(z), \tag{A 1}$$

$$N^{+} = N^{-} = -\mathrm{i}k\bar{p}^{+} - \mathrm{i}\left(ku_{00} - \omega\right), \quad L^{-} = -\mathrm{i}\left(ku_{00} - \omega\right)^{-1}\left[\frac{k^2}{\rho^{-}}\bar{p}^{-} - \mathrm{i}k\lambda^{-}N^{-}\right], \tag{A 2}$$

with the new variable $z = -\bar{Y}$ introduced for the film flow, the controlling equations and the end-point conditions are written in the form

$$\hat{v}^{+\prime\prime\prime} = \mathrm{i}\left(k\bar{Y} + ku_{00} - \omega\right)\hat{v}^{+\prime} - \mathrm{i}k\hat{v}^{+}, \quad \text{when} \quad \bar{Y} \geqslant 0; \quad \hat{v}^{+}(\infty) = \hat{v}^{+\prime}(\infty) = 0; \tag{A 3}$$

$$\left.\begin{aligned} v^{-}\hat{v}^{-\prime\prime\prime} = \mathrm{i}\left(-k\lambda^{-}z + ku_{00} - \omega\right)\hat{v}^{-\prime} + \mathrm{i}k\hat{v}^{-}, \quad \text{when} \quad a \geqslant z \geqslant 0; \\ \hat{v}^{-}(a) = -N^{-} - aL^{-}, \quad \hat{v}^{-\prime}(a) = -L^{-}; \end{aligned}\right\} \tag{A 4}$$

for the upper and lower fluids, respectively. The interface conditions are

$$\bar{p}^+ - \bar{p}^- = -\left(\gamma_0 k^2 + \frac{1-\rho^-}{Fr_0}\right)\frac{N^+ + \hat{v}_0}{\mathrm{i}\,(ku_{00}-\omega)}, \tag{A 5}$$

$$\hat{v}^+(0) = \hat{v}^-(0) = \hat{v}_0, \tag{A 6}$$

$$\varepsilon_1 = 0, \quad \varepsilon_2 = 0, \tag{A 7}$$

where

$$\left.\begin{aligned} \varepsilon_1 &= \hat{v}^{+\prime\prime}(0) - \rho^- v^- \hat{v}^{-\prime\prime}(0), \\ \varepsilon_2 &= \frac{1-\lambda^-}{\mathrm{i}\,(ku_{00}-\omega)}\left(\hat{v}_0 + N^+\right) - \frac{1}{\mathrm{i}k}\left(\hat{v}^{+\prime}(0) + \hat{v}^{-\prime}(0) + L^- - \mathrm{i}k\right), \end{aligned}\right\} \tag{A 8}$$

and $\hat{v}_0$ is the (unknown) common velocity of the two flows at the interface.

The condition $\bar{A} = 1$ was used to normalize the eigensolution, giving also $\bar{p}^+ = |k|$. To start iterations at a chosen value of the wavenumber, initial guesses are made on the complex frequency ω and on the interface velocity $\hat{v}_0$. With the constants $N, L, \bar{p}^-$ determined by (A 2), (A 5), equations (A 3), (A 4) are solved with (A 6) as two independent boundary-value problems, using a simple second-order-accurate routine. First and second derivatives of $\hat{v}^{\pm}$ are then evaluated at the interface and Newton's corrections to the frequency and interface velocity are obtained from a linearized form of (A 7).

Initial guesses are made using asymptotic solutions of §4 and 5, or from the known results for a single-fluid flow. In many cases an approximate value of the frequency and a fairly arbitrary choice for $\hat{v}_0$ were sufficient to start iterations for moderate values of the parameters, although in extreme cases, especially for large wavenumbers, parametric marching along solution curves was found necessary.

REFERENCES

Akylas, T. R. 1982 A nonlinear theory for the generation of water waves by wind. *Stud. Appl. Maths* **67**, 1–24.

Andreussi, P., Asali, J. C. & Hanratty, T. J. 1985 Initiation of roll waves in gas-liquid flows. *AIChE J.* **31**, 119–126.

Bagbekov, R. K. & Terent'ev, E. D. 1991 On one initial-value problem for a heavy viscous liquid flowing down an inclined plane. *Izv. Akad. Nauk SSSR, Mekh. Zhidk. Gaza* **5**, 90–98 (in Russian).

Beckett, P. & Poots, G. 1972 Laminar film condensation in forced flows. *Q. J. Mech. Appl. Maths* **25**, 125–152.

Belcher, S. E., Harris, J. A. & Street, R. L. 1994 Linear dynamics of wind waves in coupled turbulent air-water flow. Part 1. Theory. *J. Fluid Mech.* **271**, 119–151.

Benjamin, T. B. 1959 Shearing flow over a wavy boundary. *J. Fluid Mech.* **6**, 161–205.

Blennerhassett, P. J. 1980 On the generation of waves by wind. *Phil. Trans. R. Soc. Lond.* A **298**, 451–494.

Blennerhassett, P. J. & Smith, F. T. 1987 Short-scale waves on wind-driven water ('cat's paws'). *Proc. R. Soc. Lond.* A **410**, 1–17.

Bowles, R. I. 1995 Upstream influence and the form of standing hydraulic jumps in liquid-layer flows on favourable slopes. *J. Fluid Mech.* **284**, 63–96.

Bowles, R. I. & Smith, F. T. 1992 The standing hydraulic jump: theory, computations and comparisons with experiments. *J. Fluid Mech.* **242**, 145–168.

Brotherton-Ratcliffe, R. V. & Smith, F. T. 1989 Viscous effects can destabilize linear and nonlinear water waves. *Theoret. Comput. Fluid Dyn.* **1**, 21–39.

Bruno, K. & McCready, M. J. 1988 Origin of roll waves in horizontal gas-liquid flows. *AIChE J.* **34**, 1431–1440.

Chang, H.-C. 1994 Wave evolution on a falling film. *Ann. Rev. Fluid Mech.* **26**, 103–136.

Charles, M. E. & Lilleleht, L. U. 1965 An experimental investigation of stability and interfacial waves in co-current flow of two liquids. *J. Fluid Mech.* **22**, 217–224.

Cohen, L. S. & Hanratty, T. J. 1965 Generation of waves in the concurrent flow of air and a liquid. *AIChE J.* **11**, 138–144.

Cowley, S. J. & Wu, X. 1993 Asymptotic approaches to transition modelling. *AGARD Rep.* 793.

Craik, A. D. D. 1966 Wind-generated waves in thin liquid films. *J. Fluid Mech.* **26**, 369–392.

Feldman, S. 1957 On the hydrodynamic stability of two viscous incompressible fluids in parallel uniform shearing motion. *J. Fluid Mech.* **2**, 343–370.

Gajjar, J. S. B 1987 Fully developed free surface flows – liquid layer flow over a convex corner. *Comput. Fluids* **15**, 337–360.

Gajjar, J. S. B. & Smith, F. T. 1983 On hypersonic self-induced separation, hydraulic jumps and boundary layers with algebraic growth. *Mathematika* **30**, 77–93.

Gastel, K. van, Janssen, P. A. E. M. & Komen, G. J. 1985 On phase velocity and growth rate of wind-induced gravity-capillary waves. *J. Fluid Mech.* **161**, 199–216.

Hanratty, T. J. & Engen, J. M. 1957 Interaction between a turbulent air stream and a moving water surface. *AIChE J.* **3**, 299–304.

Hanratty, T. J. & Hershman, A. 1961 Initiation of roll waves. *AIChE J.* **7**, 488–497.

Healey, J. J. 1995 On the neutral curve of the flat-plate boundary layer: comparison between experiment, Orr–Sommerfeld theory and asymptotic theory. *J. Fluid Mech.* **288**, 59–73.

Hooper, A. P. 1985 Long-wave instability at the interface between two viscous fluids: Thin-layer effects. *Phys. Fluids* **28**, 1613–1618.

Hooper, A. P. & Boyd, W. G. 1983 Shear-flow instability at the interface between two fluids. *J. Fluid Mech.* **128**, 507–528.

Hooper, A. P. & Boyd, W. G. 1987 Shear-flow instability due to a wall and a viscosity discontinuity at the interface. *J. Fluid Mech.* **179**, 201–225.

Howarth, J. A., Poots, G. & Wynne, D. 1978 Laminar film condensation on the underside of an inclined flat plate. *Mech. Res. Commum.* **5**, 369–374.

Hoyle, J. M. & Smith, F. T. 1994 On finite-time break-up in three-dimensional unsteady interacting boundary layers. *Proc. R. Soc. Lond.* A **447**, 467–492.

Hultgren, L. S. 1992 Nonlinear spatial equilibration of an externally excited instability wave in a free shear layer. *J. Fluid Mech.* **236**, 635–664.

Kao, T. W. & Park, C. 1972 Experimental investigations of the stability of channel flows. Part 2. Two-layered co-current flow in a rectangular channel. *J. Fluid Mech.* **52**, 401–423.

Lin, C. C. 1955 *The Theory of Hydrodynamic Stability*. Cambridge University Press.

Lock, R. C. 1954 Hydrodynamic stability of the flow in the laminar boundary layer between parallel streams. *Proc. Camb. Phil. Soc.* **50**, 105–124.

Ludwieg, H. & Hornung, H. 1989 The instability of a liquid film on a wall exposed to an air flow. *J. Fluid Mech.* **200**, 217–233.

Makhmudov, A. A. & Terent'ev, E. D. 1988 Flow of a fluid down an inclined plane for large Reynolds numbers. *Prikl. Mat. Mekh.* **52**(4), 601–609 (in Russian).

Messiter, A. F. 1970 Boundary-layer flow near the trailing edge of a flat plate. *SIAM J. Appl. Maths* **18**, 241–257.

Messiter, A. F. 1983 Boundary-layer interaction theory. *Trans. ASME* E: *J. Appl. Mech.* **50**, 1104–1113.

Miesen, R. & Boersma, B. J. 1995 Hydrodynamic stability of a sheared liquid film. *J. Fluid Mech.* **301**, 175–202.

Miles, J. W. 1957 On the generation of surface waves by shear flows. *J. Fluid Mech.* **3**, 185–204.

Miles, J. W. 1959 On the generation of surface waves by shear flows. Part 2. *J. Fluid Mech.* **6**, 568–582.

Miles, J. W. 1960 The hydrodynamic stability of a thin film of liquid in uniform shearing motion. *J. Fluid Mech.* **8**, 593–610.

Miles, J. W. 1962 On the generation of surface waves by shear flows. Part 4. *J. Fluid Mech.* **13**, 433–448.

Morland, L. C. & Saffman, P. G. 1993 Effect of wind profile on the instability of wind blowing over water. *J. Fluid Mech.* **252**, 383–398.

Morland, L. C., Saffman, P. G. & Yuen, H. C. 1991 Waves generated by shear layer instabilities. *Proc. R. Soc. Lond.* A **433**, 441–450.

Neiland, V. Ya. 1969 Towards a theory of separation of the laminar boundary layer in a supersonic stream. *Izv. Akad. Nauk SSSR, Mekh. Zhidk. Gaza* **4**, 33–35 (in Russian).

Nelson, J. J., Alving, A. E. & Joseph, D. D. 1995 Boundary layer flow of air over water on a flat plate. *J. Fluid Mech.* **284**, 159–169.

Renardy, Y. 1985 Instability at the interface between two shearing fluids in a channel. *Phys. Fluids* **28**, 3441–3443.

Ryzhov, O. S. & Terent'ev, E. D. 1986 On the transition regime, which characterizes the start-up process of vibrator oscillations in a subsonic boundary layer on a flat plate. *Prikl. Matem. Mekh.* **50**, 974–986 (in Russian).

Shrira, V. I. 1993 Surface waves on shear currents: solution of the boundary-value problem. *J. Fluid Mech.* **252**, 565–584.

Shu, J.-J. & Wilks, G. 1995 Mixed-convection laminar film condensation on a semi-infinite vertical plate. *J. Fluid Mech.* **300**, 207–229.

Smith, F. T. 1979*a* On the non-parallel flow stability of the Blasius boundary layer. *Proc. R. Soc. Lond.* A **366**, 91–109.

Smith, F. T. 1979*b* Nonlinear stability of boundary layers for disturbances of various sizes. *Proc. R. Soc. Lond.* A **368**, 573–589.

Smith, F. T. 1982 On the high Reynolds number theory of laminar flows. *IMA J. Appl. Maths* **28**, 207–281.

Smith, F. T. 1986 Two-dimensional disturbance travel, growth and spreading in boundary layers. *J. Fluid Mech.* **169**, 353–377.

Smith, F. T. & Bowles, R. I. 1992 Transition theory and experimental comparisons on (I) amplification into streets and (II) a strongly nonlinear break-up criterion. *Proc. R. Soc. Lond.* A **439**, 163–175.

Smith, M. K. & Davis, S. H. 1982 The instability of sheared liquid layers. *J. Fluid Mech.* **121**, 187–206.

Stewart P. A. & Smith, F. T. 1992 Three-dimensional nonlinear blow-up from a nearly planar initial disturbance, in boundary-layer transition: theory and experimental comparisons. *J. Fluid Mech.* **244**, 79–100.

Stewartson, K. 1969 On the flow near the trailing edge of a flat plate. Part II. *Mathematika* **16**, 106–121.

Stewartson, K. 1974 Multistructured boundary layers on flat plates and related bodies. *Adv. Appl. Mech.* **14**, 145–239.

Stewartson, K. & Williams, P. G. 1969 Self-induced separation. *Proc. R. Soc. Lond.* A **312**, 181–206.

Timoshin, S. N. 1996 Receptivity problems in the weakly nonlinear stability theory at large Reynolds numbers. In *Instability and Transition in 3D Boundary Layers*, *IUTAM* Symp, pp. 399–407. Kluwer.

Tsao, J.-C., Rothmayer, A. P. & Ruban, A. I. 1997 Stability of air flow past thin liquid films on airfoils. *Comput. Fluids* (accepted); also *AIAA Paper*, 96–2155, 1996.

Valenzuela, G. R. 1976 The growth of gravity-capillary waves in a coupled shear flow. *J. Fluid Mech.* **76**, 229–250.

Yantsios, S. G. & Higgins, B. G. 1988 Linear stability of plane Poiseuille flow of two superposed fluids. *Phys. Fluids* **31**, 3225–3238.

Yih, C. S. 1967 Instability due to viscosity stratification. *J. Fluid Mech.* **27**, 337–352.

Yih, C. S. 1990 Wave formation on a liquid layer for de-icing airplane wings. *J. Fluid Mech.* **212**, 41–53.

Zhuk, V. I. & Ryzhov, O. S. 1980 Free interaction and stability of an incompressible boundary layer. *Dokl. Akad. Nauk SSSR* **253**, 1326–1329 (in Russian).